THE EFFECTS OF SOLIDIFICATION CONDITIONS ON THE FORMABILITY OF THE TWIN-ROLL CAST AA1050 STRIP

by

Kadri Can Atlı

B.S., in Mechanical Engineering, Boğaziçi University, 2002

Submitted to the Institute for Graduate Studies in
Science and Engineering in partial fulfillment of
the requirements for the degree of
Master of Science

Graduate Program in Mechanical Engineering
Boğaziçi University

2007

ACKNOWLEDGEMENTS

I would like to express my appreciation to my thesis advisor, Prof. Sabri Altıntaş, for his guidance and support throughout this project.

Special thanks to all members of the Research and Development Department of Assan Aluminyum A.Ş., especially Dr. Murat Dündar and Dr. Özgül Keleş for generously sharing their time and knowledge in this thesis. They stimulated my fascination for the discipline of materials science, which was my least favorite subject during undergraduate studies. I am indebted to the staff of the Quality System Laboratory of Assan Alüminyum A.Ş., especially Hüsnü Öztürk and Cemal Çelebi for their assistance in the conduction of the formability tests and microstructural examinations. I am also profoundly grateful to Cem Aluç and Cemal Kömeçoğlu of the mechanical workshop of Assan Alüminyum A.Ş. for their invaluable supports and advices throughout the manufacturing stages of the prototype twin-roll caster.

I would like to thank Fatih Karakoyun, my partner during my studies in Assan Alüminyum A.Ş., for his friendship and support. I would also like to express my gratitude to the assistants and colleagues at the Materials Laboratory of Boğaziçi University, especially Nazım Mahmutyazıcıoğlu, for their supports throughout the casting trials and formability tests.

Finally, I would like to thank my parents for their patience and unceasing warm supports and my brother, who has always been an inspiration and motivation for me with his wisdom and intellect.

ABSTRACT

THE EFFECTS OF SOLIDIFICATION CONDITIONS ON THE FORMABILITY OF THE TWIN-ROLL CAST AA1050 STRIP

Twin-roll casting (TRC) is a continuous sheet metal casting process, which was developed as an alternative to the conventional "ingot casting and hot mill method" of sheet metal production. Unlike the latter method, TRC combines the solidification of liquid metal and hot rolling at a single stage, thereby saving considerable energy, manpower and consumables.

In the current work, the effects of three important solidification parameters on the formability behaviour of the twin-roll cast AA1050 sheet were studied. The parameters investigated were the casting speed, the casting gauge and the diameter of caster rolls. Initially, specimens of different parameter groups were cold rolled and annealed to same thicknesses and 0 temper condition from the as-cast state. Followingly, a series of intrinsic and simulative formability tests, including the uniaxial tensile test, Brinell hardness test, Erichsen test and dome stretching tests were performed. Using grid strain analysis method on the dome stretching test specimens and the uniaxial tensile test specimens, forming limit diagram (FLD) characterization was carried out. Microstructural study was conducted on the as-cast and 0-condition samples. Within the framework of the current study, the cold rolling machine in the Materials Laboratory was revised into a twin-roll caster and casting trials were performed. The microstructure of the samples obtained from the prototype caster was compared with the typical microstructure obtained from an industrial caster.

It was observed from the test results that, changes in all three solidification parameters caused variations in formability, while the change in caster roll diameter caused the most significant changes. Moreover, test group samples cast at a small roll diameter illustrated a remarkably different microstructure, compared to the samples of the other test groups.

ÖZET

İKİZ MERDANE SÜREKLİ DÖKÜM YÖNTEMİYLE ÜRETİLMİŞ AA1050 LEVHANIN KATILAŞMA KOŞULLARININ ŞEKİLLENDİRİLEBİLİRLİĞİNE ETKİLERİ

İkiz-merdane sürekli levha döküm yöntemi, geleneksel "külçe döküm - sıcak hadde" yoluyla levha üretim yöntemine alternatif olarak geliştirilmiştir. İkiz-merdane sürekli levha döküm yönteminde katılaşma ve deformasyon aşamaları tek bir aşamada gerçekleştirilmektedir. Bu yöntem, geleneksel yöntemle karşılaştırıldığında enerji, işgücü ve sarf malzemeden tasarruf sağlamaktadır.

Mevcut çalışmada, ikiz-merdane sürekli levha döküm yönteminde önemli rol oynayan üç farklı katılaşma parametresinin, AA1050 levhasının şekillendirilebilirlik davranışına etkileri incelenmiştir. Çalışmada incelenen parametreler döküm hızı, döküm kalınlığı ve döküm merdanesi çapıdır. Farklı parametrelerde üretilen numuneler öncelikle aynı kalınlığa haddelenmiş ve ardından 0-kondüsyona tavlanmıştır. Daha sonra, bu numunelere çekme testi, Erichsen testi, gerdirme testi ve Brinell sertlik testleri uygulanmıştır. Gerdirme testi ve çekme testi numunelerinde ağ genleşme analizi yönteminden faydalanılınarak, farklı parameter gruplarının sınır şekillendirme diyagramları (SŞD) oluşturulmuştur. Numunelerin döküm hali ve tavlanmış son hallerinin mikroyapıları incelenmiştir. Çalışma kapsamında Malzeme Laboratuvarı'ndaki soğuk hadde makinası revize edilerek döküm denemeleri yapılmış; alınan numunelerin mikroyapıları, endüstriyel döküm makinasından alınan tipik numune mikroyapısı ile karşılaştırılmıştır.

Sonuç olarak, her üç parametrenin de şekillendirilebilirlik davranışına etkisi olduğu, ancak en büyük etkinin döküm merdanesi çapının değişmesiyle ortaya çıktığı tespit edilmiştir. Diğer parameter grubu numuneleriyle karşılaştırıldığında, küçük döküm merdanesi çapı ile alınan numunelerde farklı bir mikroyapı ile karşılaşılmıştır.

TABLE OF CONTENTS

LIST OF FIGURES

LIST OF TABLES

LIST OF SYMBOLS/ABBREVATIONS

A_x	Contact area between the rolled material and the roll pass
d	Indentation diameter in Brinell Hardness test
D	Ball diameter in Brinell Hardness test
e	Engineering strain
e_1	Major strain
e_2	Minor strain
F	Separating force
h	Interfacial heat transfer coefficient
k	Strength coefficient
l_o	Initial long dimension of the grid pattern
l_f	Final long dimension of the grid pattern
m	Strain rate sensitivity
n	Strain hardening coefficient
$\bar{n}$	Average value of strain hardening coefficients
P	Load in Brinell Hardness test
$\bar{p}$	The mean unit pressure on the casting rolls
r	Plastic strain ratio
r_m	Normal anisotropy
S	Engineering stress
w_o	Initial width dimension of the grid pattern
w_f	Final long dimension of the grid pattern
ε_t	True thickness strain
ε_w	True width strain
Δr	Planar anisotropy
σ	True stress

$\bar{\sigma}_{av}$	Average flow stress within the roll gap

ASTM	American Society for Testing and Materials
DC	Direct-chill semi-continuous casting
FLC	Forming limit curve
FLD	Forming limit diagram
HB	Brinell Hardness value
HRC	Rockwell Hardness value
LDH	Limiting Dome Height
TRC	Twin-roll casting

1. INTRODUCTION

Twin-roll casting (TRC) is a continuous sheet metal casting process, in which solidification and hot rolling occurs at a single step. The process involves the feeding of liquid metal to two counter rotating and internally water cooled rolls. Upon its contact with the rolls, the liquid metal is rapidly solidified, hot rolled and exits the rolls as solid sheet. With the TRC process, it is possible to cast sheets with a thickness range of 1-10 mm.

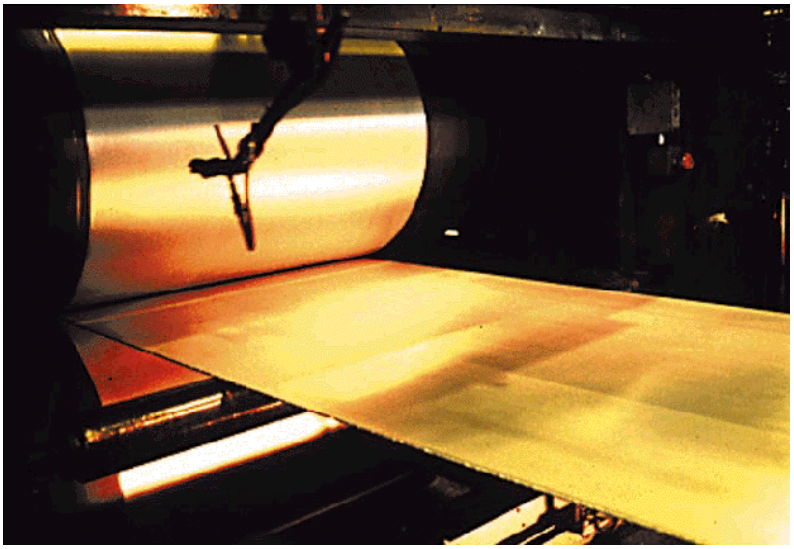

Figure 1.1. A commercial twin-roll caster [1]

The ultimate goal in TRC is to cast thinner, wider and faster while minimizing the macro and microdefects on the sheet metal. Casting wider and faster directly increases the productivity, while casting at a reduced gauge is advantageous in a way that it can save several subsequent cold rolling steps.

Since the process includes both solidification and deformation, the control of the process is inherently difficult. There are many process parameters which interact with each other. Tight control of the solidification conditions is thus a crucial requirement to prevent or significantly delay the onset of macro and microstructural defects on the sheet metal.

To date, considerable attention has been given to the effect of solidification conditions on the microstructures of TRC sheets [2-5]. Since the formability behaviour of a sheet metal is directly related to its microstructure and texture, these works were mainly limited with microstructural studies and gave little or no emphasis on the formability side of the problem, except predictions based on the microstructural characteristics.

The objective of the current work is to study the effects of three solidification parameters, namely the casting speed, casting gauge and the roll diameter on the formability behaviour of the AA1050 sheet. As-cast samples produced at different parameters are initially cold rolled to 1.5 mm and subsequently annealed to 0-condition. Followingly, a series of formability tests, including the uniaxial tension test, Erichsen test and the dome stretch test are carried out to figure out the differences in formability behaviours. Brinell hardness values are recorded to measure the resistance of samples to indentations. In addition, microstructural examinations are carried out on both the as-cast specimens and the 1.5 mm, 0-condition specimens to obtain a sound formability characterization. From the results of the uniaxial tensile test, strain hardening coefficient n, normal anisotropy r_m, planar anisotropy Δr and uniform elongation values are found for each annealed specimen cast at different solidification parameters. Erichsen test values give information about the stretchability of the annealed specimens, while dome stretch tests are beneficial in the characterization of forming limit diagrams (FLD) and calculation of the limiting dome heights (LDH).

2. LITERATURE SURVEY

2.1. Aluminum, a Material for Economic Growth

Engineering materials are of primary importance to industrial and economic growth of a country. The Gross Domestic Product (GDP) values of rapidly industrializing countries show positive correlation with the production and consumption of engineering materials such as steel, aluminum and copper. China is a perfect example for the significance of engineering materials. It showed a GDP increase of 10.4% in the third quarter of 2006 with an industrial production increase of 14.7% compared to 2005 values [6]. China is the leader of world crude steel production and accounts for 1/4 of the whole world production itself.

Aluminum is the second widely used engineering metal today after iron and steel. It has many advantages like light weight, corrosion resistance, electrical and thermal conductivity compared to iron and steel. It has frequent use in automotive/transport, construction and packaging industries.

Turkey was introduced to aluminum in 1950's. The aluminum industry became one of the leading industries in Turkey with the foundation of Etibank Seydişehir Aluminum Facilities in 1974. Turkish aluminum industry is continually progressing with its exports to EU and Middle East countries.

Presently, the annual aluminum consumption per capita in Turkey is around 3 kg. This amount is about 5-6 folds less compared to developed countries. When the advantages of aluminum usage are taken into consideration, it is easy to see that Turkey has a huge potential for aluminum usage.

Etibank Seydişehir Aluminum Facilities is the only primary aluminum producer in Turkey. (Primary aluminum production is the weight of liquid aluminum as tapped from the pots excluding alloying elements, returned scrap or remelted products [7]). Its capacity is 60,000 tons of aluminum annually. Due to this insufficiency, the production of

extrusions, flat products, castings and conductors is mainly realized by the private sector in Turkey. The annual production capacity is approximately 120,000 tons for extrusions, 100,000 tons for flat products, 75,000 tons for castings and 60,000 tons for conductors [8].

2.2. Main Aluminum Products and Applications

Aluminum semi-products and products are produced by casting and bulk deformation processes such as extrusion, rolling and drawing.

Casting methods, such as die casting, sand casting and investment casting are used to produce castings in different shapes, sizes and tolerances. Those parts are used in a variety of applications including:

- Lightweight components for vehicles, aircraft, ships and spacecraft.
- General engineering components where light weight and corrosion resistance are required.
- Architectural fittings where light weight and good appearance are important.
- High-tech products for office and home [7].

Aluminum extrusions can be made with almost any kind of cross-sectional shape. They can be further fabricated with ease by cutting, drilling, punching, machining, bending, finishing and other conventional methods. Extruded products are used throughout the construction industry, particularly in window and door frame systems, prefabricated houses and building structures, roofing and exterior cladding and curtain walling. Extrusions are also used in road and rail vehicles, airframes and marine applications [7].

The specific electrical conductivity of aluminum makes it indispensable for electronics and electrics. Aluminum cables carry twice as much current as copper of the same weight. Also, high thermal conductivity makes it very suitable for heating and cooling applications.

To obtain flat products such as sheets and foil, usually hot and cold rolling processes are used. Prior to rolling, the aluminum is in the form of an ingot which can be up to 600

mm thick. This ingot is then heated to around 500°C and passed several times through the hot rolling mill (Figure 2.1). This gradually reduces the thickness of the metal to around 6 mm [7].

This thinner aluminum is then coiled and transported to the cold rolling mill for further processing. There are various types of cold rolling mills, and they produce various types of rolled products, with thicknesses as low as 5 µm. In general the type of product depends on the alloy used, the rolling deformation and thermal treatment used in the process as well as careful adjustments to the mechanics and chemistry of the process. Rolling mills are controlled by very precise mechanisms and measuring systems [7].

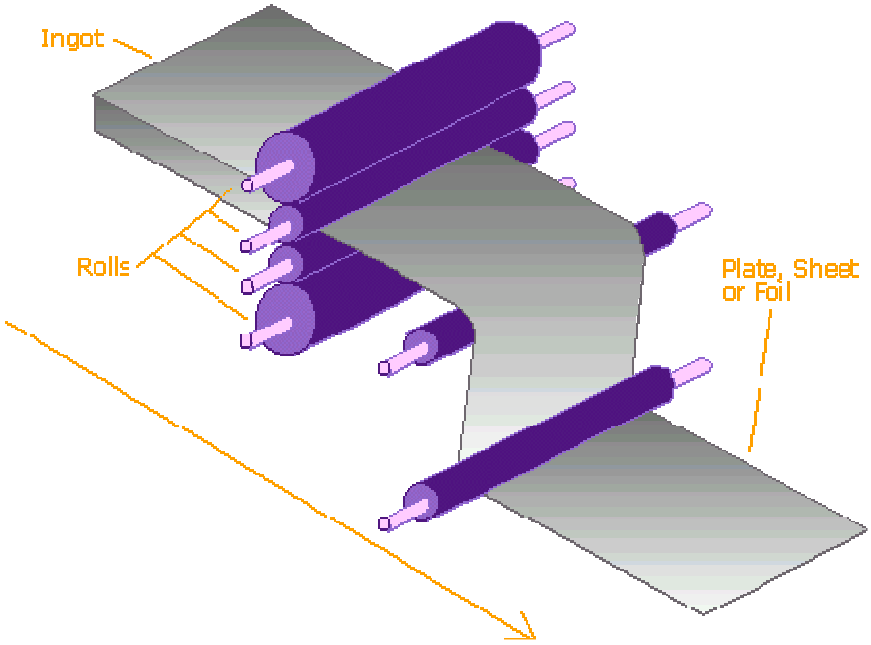

Figure 2.1. Sheet production with the hot rolling process [7]

Rolled products can be classified as foil, sheet and plate:

Foil is less than 0.2 mm thick and is used mainly in the packaging industry for foil containers and wrapping. Foil is also used for electrical applications, building insulation and in the printing industry [7].

Sheet is between 0.2 mm and 6 mm in thickness and has a wide variety of uses in the construction industry including aluminum siding and roofing. Sheet is also used extensively in transport applications such as automobile body panels, airframes and the hulls of boats [7].

Plate is any rolled product over 6 mm in thickness. It also be found in a number of applications including airframes, military vehicles and structural components in bridges and buildings [7].

2.3. Alloy Designation and Temper Convention of Aluminum

Aluminum alloys are available as wrought products, ingots for casting and powder for powder-metallurgy applications.

Wrought aluminum alloys can be classified as:

- alloys that can be hardened by cold-working and are not heat-treatable,
- alloys that can be hardened by heat treatment [9]

Non heat-treatable aluminum alloys cannot be precipitation-strengthened but can only be cold-worked to increase their strength. Their strength roots from solute hardening mechanism with the alloying elements.

2.3.1. Alloy Designation System

Wrought-aluminum alloys are identified by four digits and by a temper designation that shows the condition of the material. The major alloying element is identified by the first digit. Here is the system [9]:

1xxx – commercially pure aluminum – excellent corrosion resistance; high electrical and thermal conductivity; good workability; low strength; not heat treatable.

2xxx – copper – high strength-to-weight ratio; low resistance to corrosion; heat treatable

3xxx – manganese – good workability; moderate strength; not generally heat-treatable

4xxx – silicon – lower melting point; forms an oxide film of a dark-gray to charcoal color; not generally heat treatable.

5xxx – magnesium – good corrosion resistance and weldability; moderate to high strength; not heat-treatable.

6xxx – magnesium and silicon – medium strength; good formability, machinability, weldability, and corrosion resistance; heat treatable.

7xxx – zinc – moderate to very high strength; heat treatable.

8xxx – other element [9]

9xxx – unused series

The second digit in these designations indicates modifications of the alloy. For the 1xxx series, the third and fourth digits stand for the minimum amount of aluminum in the alloy – for example, “1050” indicates a minimum of 99.50% aluminum, “1090” indicates a minimum of 99.90% aluminum. In other series, the third and fourth digits identify the different alloys in the group and have no numerical significance [9].

2.3.2. Temper Convention

Temper designations for wrought aluminum alloys follow the alloy designation and are separated by a hyphen (for example 1100-0). Subdivisions of a basic temper are indicated by one or more digits and follow the letter of the basic designation (for example, 1100-H14) [10].

Basic temper designations are as follows:

F – As fabricated. No control over the amount of strain hardening; no mechanical property limits.

O – Annealed and recrystallized. Temper with the lowest strength and highest ductility.

H – Strain-hardened

T – Heat-treated to produce stable tempers other than F or O [10].

Following is the designation system for the strain-hardened subdivisions:

H1 – Strain-hardened only. The degree of strain hardening is indicated by the second digit and varies from quarter-hard (H12) to full-hard (H18), which is produced with approximately 75% reduction in area.

H2 – Strain-hardened and partially annealed. Tempers ranging from quarter-hard to full-hard obtained by partial annealing of cold-worked materials with strengths initially greater than desired. Tempers are H22, H24, H26 and H28.

H3 – Strain-hardened and stabilized. Tempers for age-softening aluminum-magnesium alloys that are strain-hardened and then heated at a low temperature to increase ductility and stabilize mechanical properties. Tempers are H32, H34, H36 and H38 [10].

The designation system for the heat-treated subdivisions is specified as:

T1 – Naturally aged. Product is cooled from an elevated-temperature shaping process and naturally aged to a substantially stable condition.

T3 – Solution heat-treated, cold worked, and naturally aged to a substantially stable condition

T4 – Solution heat-treated and naturally aged to a substantially stable condition.

T5 – Cooled from an elevated-temperature shaping process and then artificially aged.

T6 – Solution heat-treated and then artificially aged.

T7 – Solution heat-treated and stabilized

T8 – Solution heat-treated, cold-worked, and then artificially aged [10].

2.4. Methods of Aluminum Sheet Production

With the introduction of aluminum in the automotive industry, manufacturers were able to improve vehicle fuel economy and reduce CO_2 emissions. The advantage of aluminum over competitive materials is its very attractive combination of low density, high strength and formability, ease of recycling, and high corrosion resistance [11].

While the application of aluminum die-cast parts is extensive, the use of aluminum sheet is relatively restricted. The major barrier to the widespread use of aluminum sheet in automotive applications is its high cost, which is four to five times that of steel sheet [11].

At present, there are two different methods to produce aluminum sheet. The first method involves the production of aluminum blocks by the direct-chill casting (DC casting) method and subsequently hot rolling and cold rolling these blocks in several passes to achieve the final sheet dimensions. The second method is TRC method, which combines both the solidification and rolling in a single step, and is capable of directly producing aluminum sheet from the melt with thicknesses of 1-10 mm.

Each of these methods has its advantages and disadvantages. Microstructural properties, initial investment costs, technological limitations with respect to the product range and productivity are some of the areas in which these two methods differ and will be briefly explained in the current work..

2.4.1. Direct-Chill Casting, Hot and Cold Rolling

The starting stock for most rolled products is the direct-chill cast ingot. The size of the ingot depends on the size of the DC unit available, the hot rolling mill capacity, volume required for a particular end use and to some extent the alloys being cast. Ingots up to over 20 tons in weight, 500-600 mm thick, 2000 mm wide and 8000 mm can be produced [12]. Figure 2.2 is an illustration of the DC casting process. The key operating requirement in DC casting is that a sufficiently strong shell be developed in the limited time of contact with the mold to retain the interior molten pool. Withdrawal rates of up to 0.2 m/min (0.66 ft/min) can be achieved in conventional casters. Pure aluminum or dilute alloys are easier to cast than higher alloys with wide freezing ranges. Higher casting speeds have led to problems in maintaining casting shape and have also caused higher internal stresses in the solidified ingot. Control of heat extraction rates is required to limit the extent of these difficulties [13].

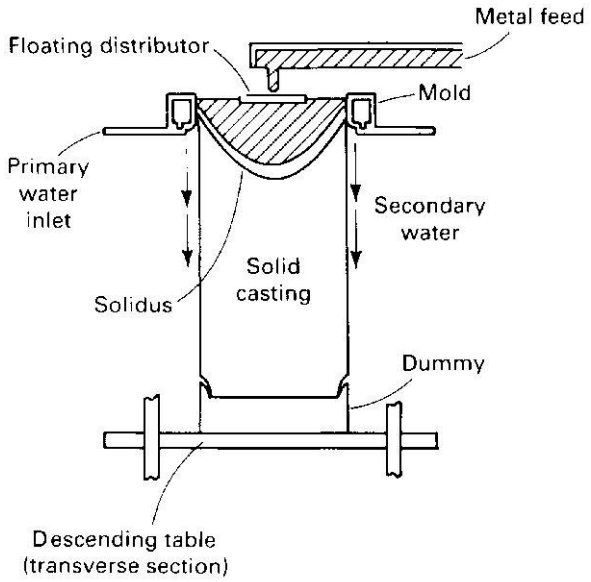

Figure 2.2. A schematic of the DC casting process [13]

The DC ingot is usually cooled after casting to room temperature and then reheated to around 500°C prior to successive passes through a hot rolling mill where it is reduced in thickness to about 4-6 mm. The strip from the hot rolling mill is coiled for transport to the cold mill which might be on the same site or elsewhere. Cold mills, in a wide range of

types and sizes are available; some are single stand, others 3 stands and some 5 stand. Cold rolling speeds vary but modern mills operate at exit speeds as high as 3000 m per minute and alloys may be cold rolled to thickness of around 0.05 mm [12].

2.4.2. Twin-Roll Casting and Cold Rolling

Unlike the DC casting and hot-rolling route of sheet metal production, TRC combines solidification and hot rolling in a single step. The liquid metal is fed through a ceramic nozzle into the bite of a 2-hi mill where the rolls are designed to fill both a heat exchanger and a rolling function (Figure 2.3). The rolls are usually comprised of two parts: a core and a shell shrink-fitted on the core. Water circulates between the core and the shell to cool the shell, which is the part in contact with the metal. The metal exiting the tip solidifies on the rolls into a strip that is further work-hardened by the rolls. To prevent the metal from sticking to the rolls a release agent (most of the time a suspension of water with graphite) is applied the rolls. This release agent acts both as a lubricant and as a thermal barrier that controls the heat exchange between the rolls and the metal [14].

The product of a twin-roll caster is a sheet which is close to the final gauge and therefore needs no further hot rolling unlike in the DC casting method; ideally only cold rolling to final gauge will be required.

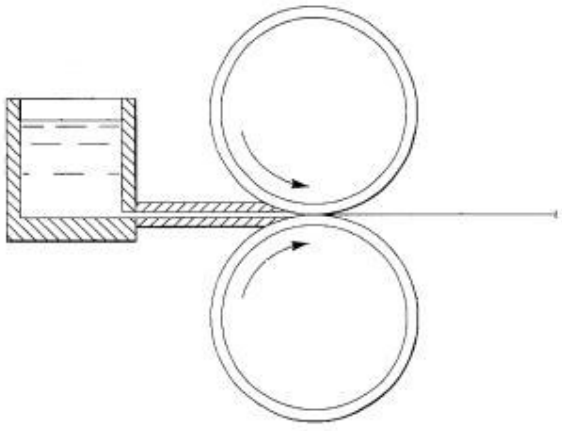

Figure 2.3. A simplified schematic of the TRC process [15]

2.4.3. Comparison of the Two Methods

A key difference between twin-roll casting and DC casting is the solidification rate of the metal. While the solidification rate in DC casting is limited to 1 to 50°C/s, it can reach 1000°C on some commercial twin-roll casters. This rate of solidification combined with the deformation produces very different microstructures to those seen in DC casting. TRC alloys usually exhibit high concentration of alloying elements in solid solution, fine primary intermetallic particles and fine as-cast grain size. All these features affect alloy response to thermomechanical treatment before and during cold rolling (homogenisation and interannealing respectively) involved in the downstream processing. Therefore, the microstructure of sheets issued from TRC and DC cast alloys can differ markedly. The differences in microstructure and in crystallographic texture have great impact on sheet mechanical properties and formability.

Slamova, M., et al. [11] have compared the materials (1.0 mm thick in the soft condition) prepared by both methods and investigated that they exhibited different microstructures. Second-phase particles were coarser and less numerous in DC cast sheets (Figure 2.4), while the grain size in TRC sheets was of the same magnitude or finer than in DC cast sheets (Figure 2.5) [11].

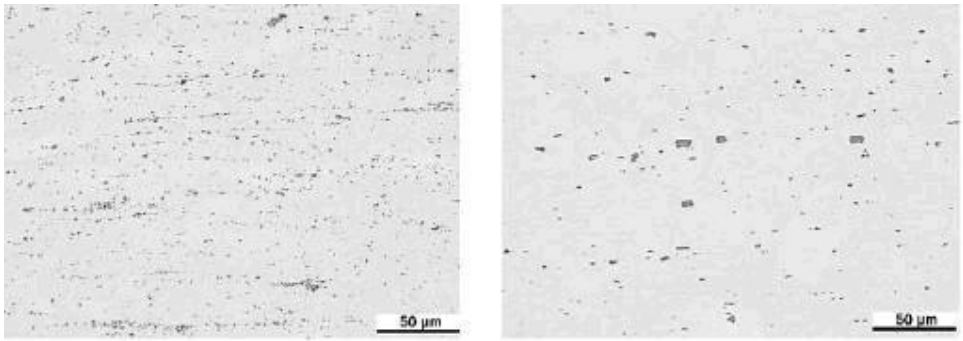

Figure 2.4. Light micrographs of second-phase particles. Sections are parallel to the rolling direction. (a) AA5052 TRC-cast sample, (b) AA5052 DC-cast sample [11]

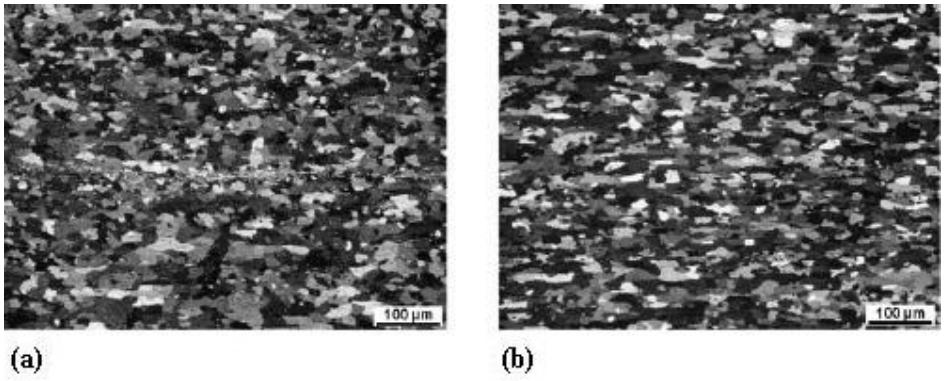

Figure 2.5. Polarized light micrographs of grain structure in mid-thickness of sheets Sections are parallel to the rolling direction. (a) AA5052 TRC-cast sample, (b) AA5052 DC-cast sample [11].

The particle distribution in the twin-roll cast sheet is non-uniform, having a concentration of coarse particles at the centerline of the strip. It should be noted, however, that the size of these coarse centerline particles is less than the mean particle size in the DC cast material. The concentration of these particles on the centerline has not been observed to have any harmful effects [5]. The fairly low exit temperature of the cast strip (approximately 300ºC) does not allow full re-crystallization to occur during hot (warm) rolling. This results in the cast strip having some residual worked structure, it is thus slightly harder than conventionally hot mill material (Figure 2.6) [5].

The differences in microstructure between twin-roll cast strip and conventional DC ingot and hot mill material require adjustment of the downstream rolling and annealing practices; twin-roll cast metal will frequently require an extra annealing cycle to obtain satisfactory final gauge properties (particularly if the final product will be deep drawn) [5].

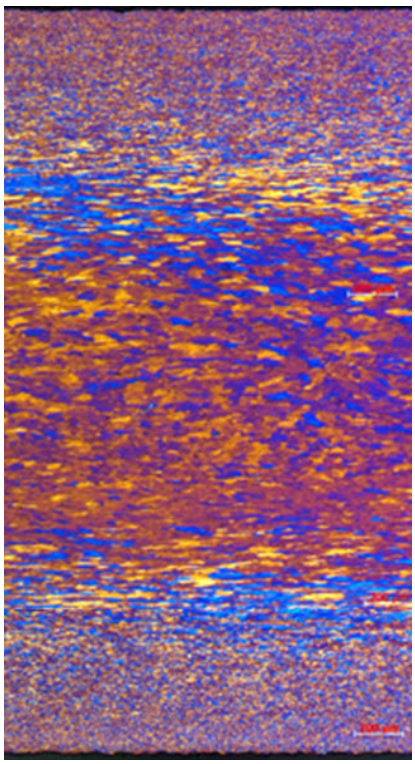

Figure 2.6. 3 mm twin-roll cast AA1050 alloy in as-cast condition. Section is parallel to the rolling direction

As previously mentioned, the twin-roll casting process converts molten aluminum directly into thin cast strip suitable for cold rolling; thus effectively eliminating the ingot casting, sawing, scalping, reheating and hot rolling associated with the traditional DC ingot and hot mill method of production. A detailed study performed by the German Metallurgical Institute shows that twin-roll casting not only significantly reduces the capital investments required (Figure 2.7), it also produces considerable savings in energy, consumables and manpower, thus reducing the producers conversion cost (Figure 2.8). These economic benefits give roll caster based plants a pricing advantage in the increasingly competitive world aluminum market [5].

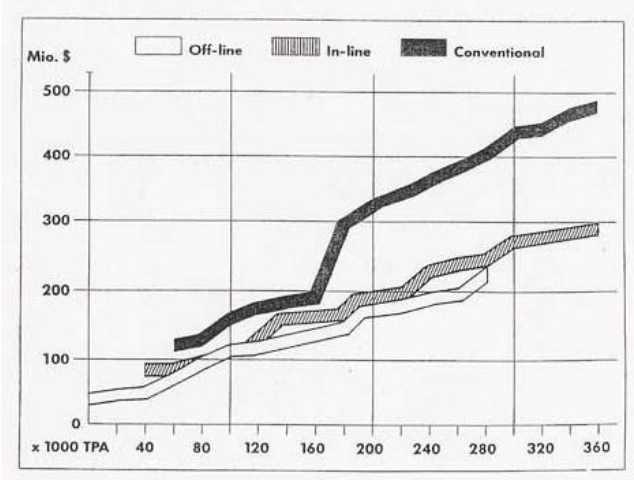

Figure 2.7. Comparison of total investment cost in 1988 U.S. $ between conventional DC ingot and hot mill method (Conventional), thick strip Hazelett/Alusuisse II Method (in-line) and the twin-roll approach (off-line) [5].

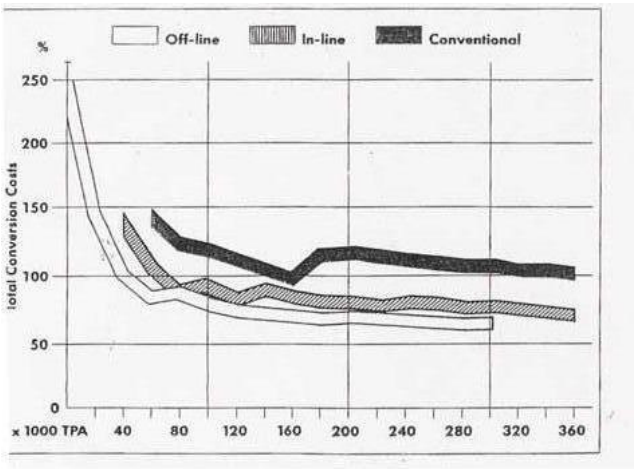

Figure 2.8. Relative conversion cost comparison between conventional DC ingot and hot mill method (Conventional), thick strip Hazelett/Alusuisse II Method (in-line) and the twin-roll approach (off-line) [5]

It is therefore envisaged that twin-roll casting of aluminum alloy sheet can compete favorably with the current processing combination of DC casting and hot rolling, resulting in significant cost benefits due to abovementioned reasons. This will have a substantial impact on the processing of aluminum alloys for foil stock, fin stock, architectural sheet and many other applications.

As compared to the DC casting and hot rolling route of sheet metal production, TRC has lower productivity values. The first reason for this is that the process is inherently much harder to control since it involves both solidification and deformation at the same time. For a quality sheet free of surface defects, the optimization of many solidification parameters is required. A slight change of these parameters during the process may cause the formation of the defects on the sheet surface and may even cause the termination of the whole process. The second reason is the limitation of the solidification rate. The primary method for increasing the productivity values is to increase the casting speed of the twin-roll caster. However, the speed can be increased just upto a value, above which the liquid metal will not be fully solidified. The current trend to solve this problem is to develop new materials with better thermal conductivity values for the caster shells. There are several studies about rolls made from copper as an alternative to the steel rolls [16, 17].

The theoretical productivity value of today's commercial twin-roll casters is about 4.96 kg/s.m. However, this value is far from reality and in practice, a productivity value of 0.248-0.372 kg/s.m can be achieved [18].

Only alloys with a narrow solidification range can be successfully produced with the twin-roll casting method. As the amount of alloying elements in the aluminum increases, the solidification range of the alloy increases, too. Harder alloys with higher levels of alloying elements and hence larger freezing ranges are more prone to surface defects during casting. Precipitation hardening alloys like AA6016, AA6061 and AA6082 are among the hardest to cast with the TRC method. Figure 2.9 illustrates the solidification ranges of some of the aluminum alloys. 2xxx and 7xxx series have the widest solidification ranges. For instance, AA2024 and AA7075 alloys which have extensive use in the aircraft industry can not be produced with the TRC method.

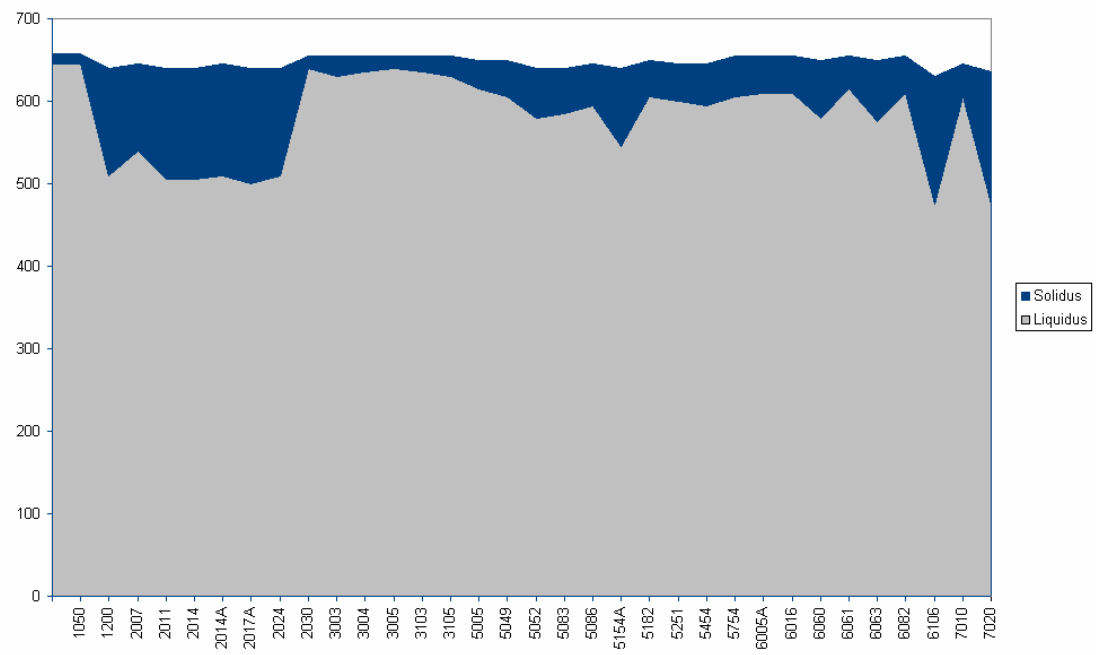

Figure 2.9. Solidification ranges for various wrought aluminum alloys

2.5. Twin-Roll Casting Process

The continuous casting of metals with the TRC process dates back to 1856 [19]. It was Sir Henry Bessemer who first invented the first twin-roll caster very similar to today's commercial casters. However, the TRC method did not see much use until 1950's due to the technological limitations experienced (e.g. control mechanisms, filtering systems, metal delivery systems). The first successful and commercial use of twin-roll casters was realized by the Hunter Engineering Co. in 1956 [20]. Presently, twin-roll casters are widely used in the aluminum industry especially in Europe and North America.

2.5.1. Overview of the Process

Figure 2.10 can be illustrated as a typical view of an entire twin-roll casting line. The line begins at a furnace on an upstream end and terminates in a coil winder on the downstream end. Raw materials (ingots, scraps, etc.) melt within the furnace are poured into a holding chamber which maintains the molten metal at a preferred temperature. Additional alloying elements are added to the melt in the holding furnace to obtain the required alloy composition.

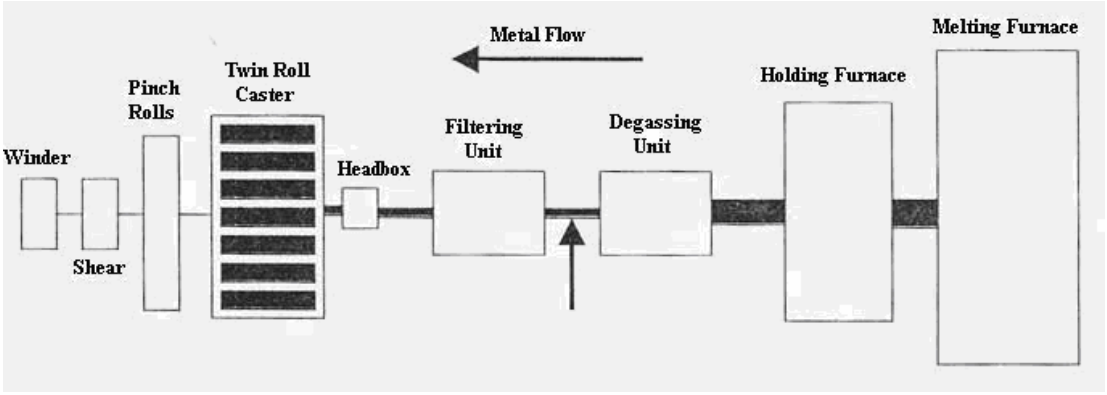

Figure 2.10. A schematic of an entire twin-roll casting line [18]

After the holding chamber, molten aluminum of a constant composition and at a constant temperature and level passes through a degassing unit, a filtering unit and a preheater (not shown in Figure 2.10) before being introduced into a headbox just prior to the twin-roll caster. The headbox is connected to a planar pouring nozzle or feed tip, which distributes the metal between the casting rolls of the twin-roll caster, the width of the tip determining the width of the cast strip (Figure 2.11). The entire frame of the twin-roll caster may be tilted with the use of hydraulic cylinders. The 15-degree tilt of the twin-roll caster allows regulation of the feed tip exit pressure by control of the headbox level, permitting smooth flow of the metal from the feed tip to the internally water cooled rolls [21].

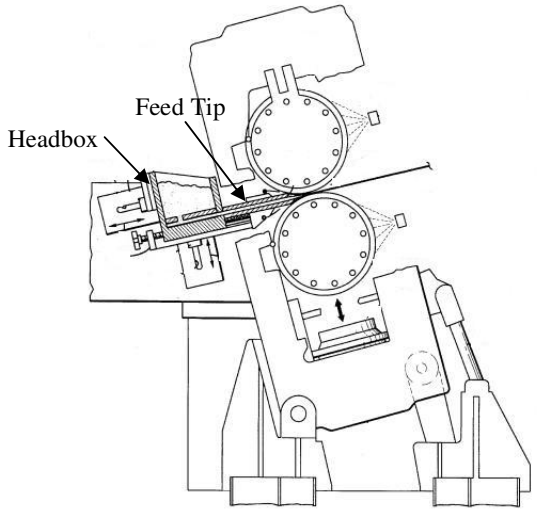

Figure 2.11. A side view of the twin-roll caster [21]

The molten metal is cast in a bite between the casting rolls and the resulting solidified strip moves over a guide-out roll, past a strip air cooler and between a set of pinch rolls. The strip then passes through a shear and finally reaches the mandrel where it is wound onto a core into a coil. When the maximum coil diameter has been reached, a coil car platen (not shown in Figure 2.10) with rollers removes the coil [21].

As seen in Figure 2.11, the twin-roll caster generally comprises the two independently driven horizontal rolls, an upper roll and a lower roll, which are internally water cooled and positioned one above the other in the frame at a 15-degree tilt. The caster frame consists of two heavy cast steel housings cross-tied for rigidity. The frame assembly is mounted for tilt-back casting position during operation with hydraulic cylinder pivot actuation to a vertical position for roll change. The caster roll shell is cooled by contact with water flowing in machined circumferential grooves in the surface of the core [21].

2.5.2. Casting Rolls

The casting rolls in the TRC process have two roles. First, they act as a heat exchanger extracting the heat of the liquid metal and carrying away this heat out of the system with the cooling water circulating in the grooves of the roll core. Second, they perform the hot rolling process after the solidification has initiated.

During casting, the roll shell is alternately subjected to high temperatures due to contact with the molten metal and then to cooling by cooling water. This results in the formation of heat cracks due to thermal fatigue on the surface of the shell which gradually penetrate deeper into the shell, causing marks on the cast strip and eventually breaking the shell. Thus, the roll shell must have an improved resistance to heat cracking. This is realized by choosing a material with a combination of low coefficient of thermal expansion, high elevated temperature yield strength, high elevated temperature ductility and a low elevated temperature modulus of elasticity.

Furthermore, to extract the heat from the liquid metal, the material must also have excellent thermal conductivity. If a material with low conductivity is to be used, the

productivity values will be lower since the time for the liquid metal to solidify will be longer, therefore requiring lower casting speeds.

Unfortunately, no known alloy system exhibits this combination of properties, and attempts to improve one of the properties in a particular alloy system usually results in the sacrifice of another. For example, an increase in yield strength typically results in a decrease in ductility in a steel alloy. Substitution of a copper base alloy would result in much higher thermal conductivity and a lower modulus of elasticity (both of which are desirable), but the coefficient of thermal expansion is high and the yield strength is low. Similar problems arise with respect to austentitic stainless steels [22].

As is well known, the thermal conductivity of steel degrades as the content of alloying elements increases, so a roll shell for use in continuous casting must be made of a material which has a relatively small amount of alloying elements and exhibits improved resistance to heat cracking during casting [23].

The standard alloy steel now used for roll caster shells comprises, in weight percent, from 0.53% to 0.58% carbon, 0.45% to 0.65% manganese, 0.20% to 0.30% silicon, about 0.02% maximum phosphorus, about 0.02% maximum sulfur, 0.40% to 0.50% nickel, 1.0% to 1.2% chromium, 0.45% to 0.55% molybdenum, 0.10% to 0.15% vanadium and balance essentially iron [22].

2.5.3. Solidification Mechanisms

Solidification can be subdivided into three areas controlled by different parameters at each area (Figure 2.12):

At the first area, liquid metal is rapidly solidified as it touches the caster rolls and a metal surface skin forms on the shells. At the second area, the core of the metal becomes semi-solid and shrinks, causing the skin to lose contact with the roll. This results in reduced heat transfer and intergrannular surface remelting. At the third area, the metal becomes fully solid and exerts pressure on the casting rolls, increasing heat transfer and removing the majority of the heat from the solidifying metal [5].

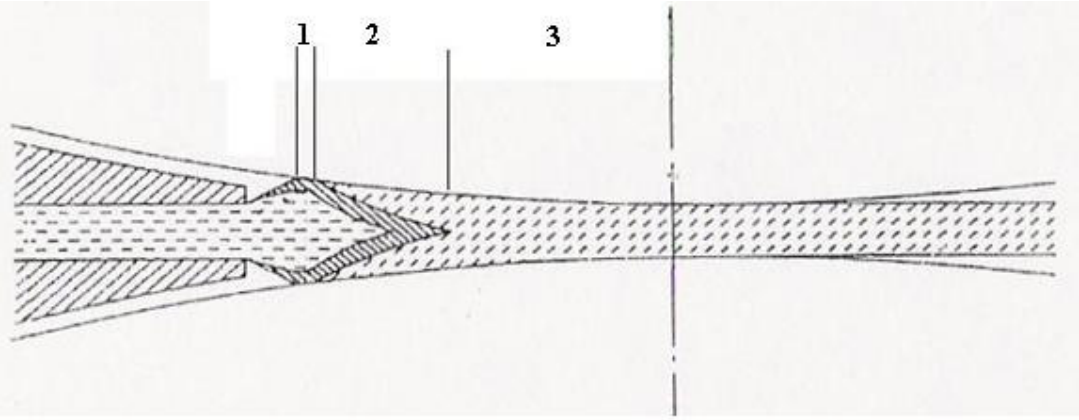

Figure 2.12. Casting region of the TRC process [5]

The remelting that occurs in the second step not only produces large intermetallics, it also causes localized oxide growths on the rolls which nucleate remelting on subsequent roll revolutions. During extended operation, the oxide areas on the roll surfaces tend to develop a cyclic pattern, causing transverse bands of coarse structure on the cast strip surface. These bands are industrially known as “ripple” and traditionally prevented roll cast strip from being used for certain anodizing applications [5].

2.5.4. Solidification Parameters

The solidification parameters can be classified as constant parameters which cannot be changed and variable parameters which can be changed during the casting process (Figure 2.13).

Constant Parameters:

- Diameter of the rolls,
- The casting roll and metal interfacial heat transfer coefficient,
- Design of the metal delivery system,

Variable Parameters:

- Casting speed,
- Tip setback,
- Casting gauge,
- Temperature and level of the metal in the headbox,
- Lubrication and cooling of the rolls.

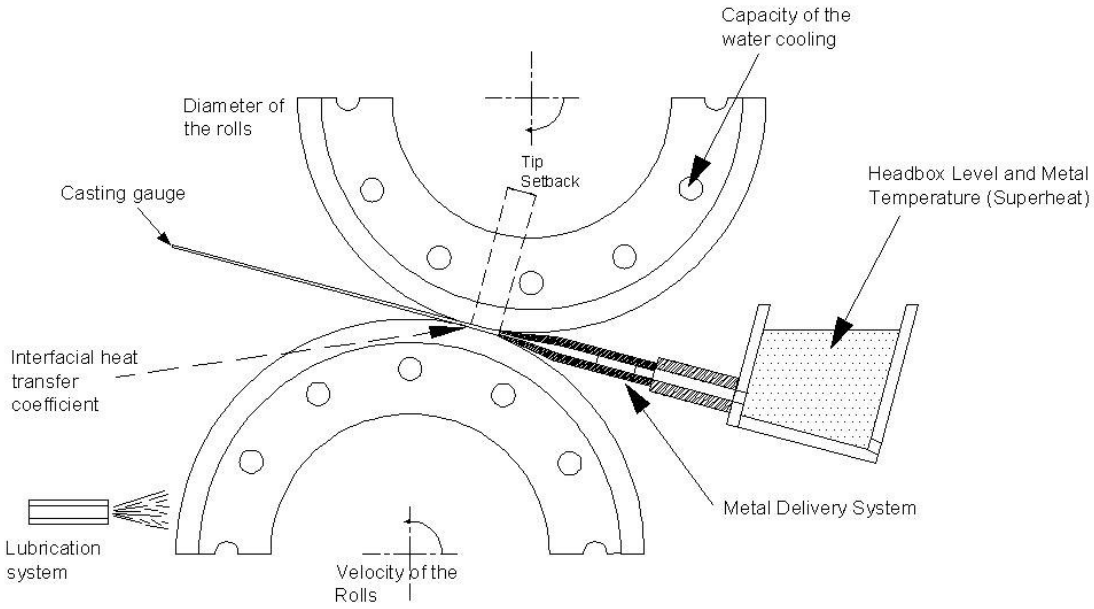

Figure 2.13. Solidification parameters in the TRC process

Figure 2.14 illustrates a 2D view of the TRC process. The ceramic tip is positioned between the rolls, such that the clearance between the edge of the tip and the roll is 0.2 mm. The molten metal leaving the ceramic tip forms the meniscus at its first contact with the rolls. The molten metal is rapidly solidified and hot worked up to the roll bite region (the region where the rolls are closest to each other). It can be seen from Figure 2.14 that as the diameter of the rolls increase, the length of the contact arc will increase to satisfy the 0.2 mm clearance between the ceramic tip and the rolls. This will provide more uniform deformation and more time for the metal to solidify.

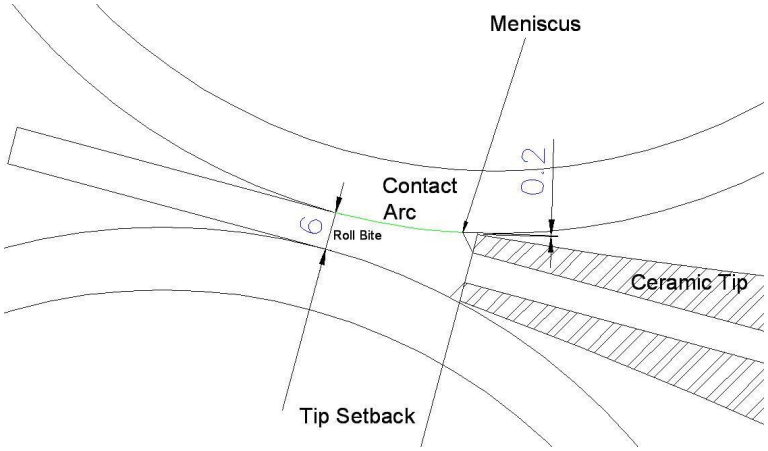

Figure 2.14. The arc of contact of liquid metal with the casting rolls

Dündar, M., et al. [24] compared the size and distribution of intermetallic particles formed through the thickness of AA 3003 strips, produced from two casters having different caster roll diameters. They concluded that the segregation behaviour of this alloy was not significantly influenced by the caster roll diameter. They also investigated that the grain size in the core of both samples was found to be at least an order of magnitude larger with respect to that at the surface.

The interfacial heat transfer coefficient (h) between the rolls and the liquid metal plays a crucial role in determining the overall productivity of the TRC process and the quality of the product. The interfacial heat transfer depends on several parameters: the conductivity of the roll material, the surface roughness of the rolls, the type of the alloy used in the casting, the cooling capacity of the rolls, lubrication of the rolls. It is desired that, the rolls should have a high thermal conductivity value to remove the heat from the molten metal as quickly as possible. The surfaces of the rolls should also be as smooth as possible to minimize the gap formation between the initially solidified strip and the roll surface.

The type of alloy being cast has a significant effect on the interfacial heat transfer coefficient. Different alloys have different conductivity values. In addition, as the amount of alloying elements increase, the solidification range of the alloy increases, making it more difficult to cast with the TRC method. As obvious from Figure 2.9, heat treatable alloys 2xxx and 7xxx have the widest freezing ranges and are among the most difficult, if

impossible to cast alloys with TRC. Also very important is the amount of latent heat the alloy can store and its ability to conduct it to the rolls (thermal diffusivity).

By taking the other process parameters constant, the effect of interfacial heat transfer coefficient on the process was simulated using the finite element method software Calcosoft 2D. Figures 2.15 and 2.16 below illustrate the solid fraction values for different h values. The mushy zone (liquidus-solidus region) is visible in the roll gap area, where transition from liquid metal (white color) to solidified strip (blue color) occurs. One can well see the influence of the heat transfer coefficient on these results. As *h* increases, the rate of solidification increases and the mushy zone moves backward towards the tip opening. Conversely, with a low h value, the mushy zone is more towards the roll bite (where the roll clearance is minimum).

It is desired that, the mushy zone should not exceed the roll bite and also not to stay far back towards the tip opening. In the former, the strip will leave the rolls partially molten, not fully hot rolled. In the latter, the strip will be excessively hot rolled leading to increased separating forces on the rolls.

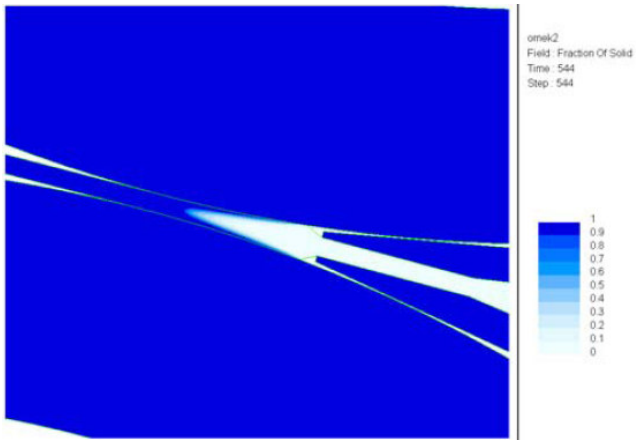

Figure 2.15. 2-D illustration of fraction of solid contours in TRC. (*h*=7500 kW/mºK)

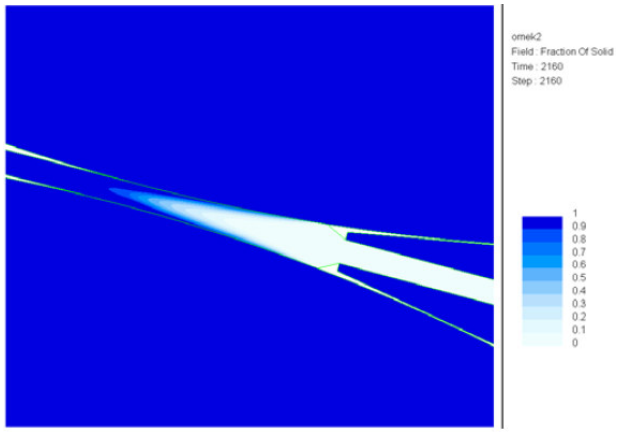

Figure 2.16. 2-D illustration of fraction of solid contours in TRC. (h=5000 kW/m°K)

The speed of the TRC process is mainly controlled by the angular velocity of the casting rolls. The liquid metal level in the headbox and the casting gauge are also effective on the casting speed, but they are dependant variables. The headbox level is adjusted according to the velocities of the rolls. It is not independantly raised or lowered to speed up or slow the process. Similarly, when the casting gauge is decreased, the casting speed is automatically increased, as long as the headbox level stays the same.

The upper limit of the casting speed, in terms of tons/hr, is defined by the volumetric flowrate of the molten metal entering the metal delivery system. The cooling capacity of the rolls (roll material, water cooling capacity, roll lubrication), the type of the alloy used in casting and the distribution of the liquid metal to the roll gap are also constraints to the casting speed. It is for this reason that for alloys with high solidification ranges (like 6xxx series), the maximum speed is low compared to lean alloys with short solidification ranges (like 1xxx series).

Figure 2.17 shows a plot of metal temperature vs angular velocity of the rolls at the roll bite. All other process parameters kept constant, the plot shows that as the velocity increases, temperature of the metal also increases. This is obvious, since the rolls will have less contact time with the molten metal and be able to extract less latent heat. On the other hand, as the velocity drops below a specific value, temperature increases again. This results from the cooling capacity of the rolls. As the velocity decreases, rolls will accumulate so much heat, that cooling water will not be able to carry away the excess heat. It would not

be correct to call this specific value as an optimum value, since this value is the minimum temperature, thus the highest separating forces. The optimum value is dependent on the type of alloy used. The angular velocity can be increased as long as the strip does not leave partially molten.

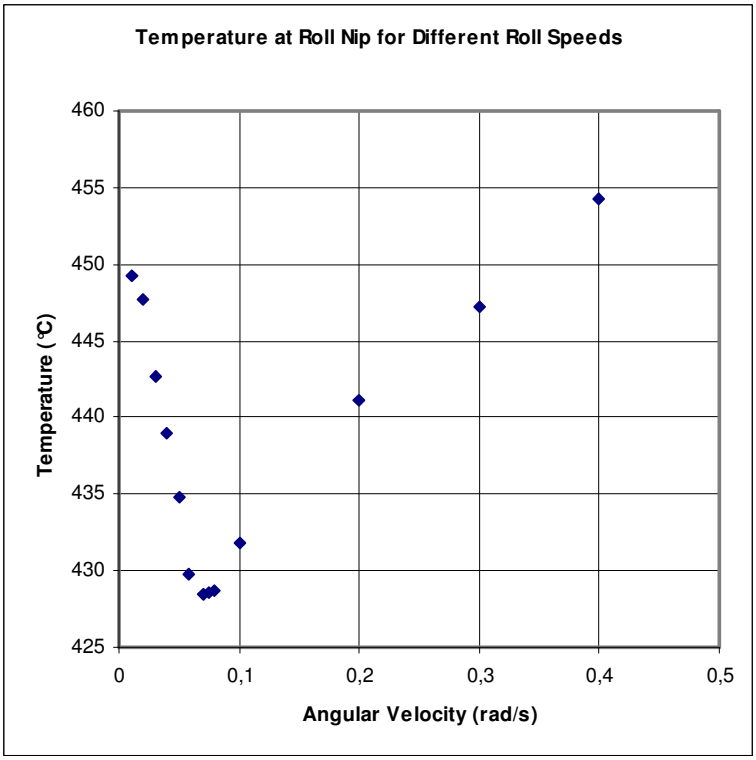

Figure 2.17. Temperature vs. roll angular velocity plot at the roll bite

Ertan, S., et al. [3] found out that the intensity of segregation increased with increasing casting speeds for a given casting gauge. The thickness of the strip which could be cast without segregation decreased with increasing casting speeds. Finally, it is confirmed that with increased casting speed (at constant strip thickness), a less deformed microstructure is developed.

Tip setback is defined as the distance between the tip of the casting nozzle and the roll nip (Figure 2.14). Setback directly affects the contact length of the molten metal with the cooling rolls. A small setback value decreases the contact length, thus decreases the amount of hot work and consequently decreases the roll separating force. It can also be concluded that a high value of setback will decrease the life of the casting rolls.

For production of high quality foil, it is critical that the tip does not rub against the casting roll. The result of this is a marking of the sheet surface and localized variations in the microstructure of the sheet. The most common method for achieving the minimum setback on the majority of casters in the world is the operator's eye. If the setback is too small, characteristic scratch marks become apparent on the sheet surface. This will prompt the operator to modify the setback slightly, until the sheet surface is scratch free.

The quality of the metal delivery system is crucial in terms of establishing a uniform liquid metal flow and temperature distribution across the orifice of the casting nozzle. This will also ensure an optimized solidification front.

The primary role of the metal delivery system is the distribution of the molten metal. The molten metal entering the casting nozzle from a narrow inlet (about 0.1m) has to be distributed to a width of about 1.5 – 2m. This is realised with using a plurality of baffles as shown in Figure 2.18. This distribution has to be done as uniformly as possible to prevent temperature and velocity differences across the width of the nozzle. Non-uniform metal distribution causes differences in the solidification behaviour of the metal, causing defects on the surface of the cast strip, like segregations and bleed-outs.

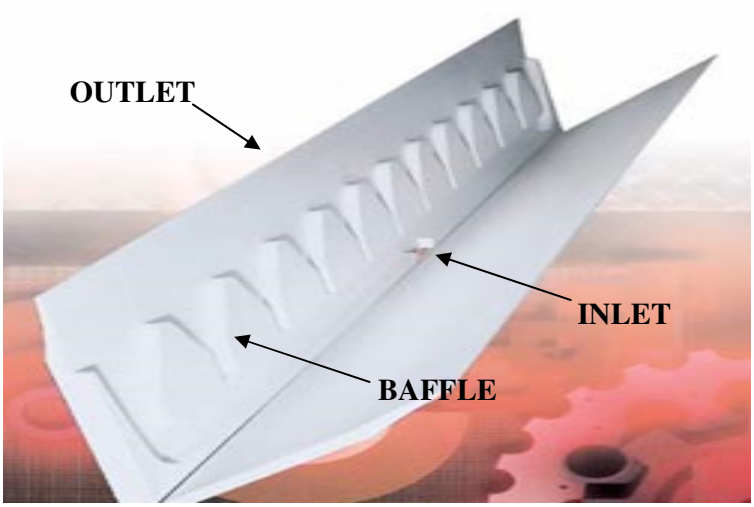

Figure 2.18. Metal delivery system used in twin-roll casting [25]

Large variations in the as-cast structure can be obtained when the gauge is reduced and the casting speed (or productivity) is increased. A gauge reduction in general results in

the deformation getting more inhomogenously distributed over the strip thickness due to a larger separating force giving enhanced hot deformation in the surface region [4].

The popular opinion of thin strip casting is that casting at thinner gauges result in a higher solidification rate thereby giving a refined metallurgical structure with smaller eutectic particles. Investigations of a large amount of samples cast at different "thin gauge conditions" have shown that this is not necessarily the case. When samples cast at 6mm are compared to thinner samples, it is observed that thinner samples have larger dendrite arm spacings (DAS), which means that microstructure solidifies with reduced cooling rate [4].

Berg, B.S., et al. [26] investigated the microstructural variations and development from the as-cast state through cold rolling and annealing of a twin-roll cast AA5052 alloy as a function of casting speed and gauge reduction. By optical characterization, they found considerable difference in the as-cast structure due to a gauge reduction from 5mm to 1.9mm, and the cooling rate was reduced in the thinner strip.

It is well known that high superheat leads to coarse, columnar grain structure, which is not good for following forming processes like rolling or extruding. Therefore, the casting temperature should be as low as possible resulting in a fine, equiaxed grain structure. The reason for it is the number of nuclei, low superheat leads to a higher under cooling and hence to a higher number of nuclei, therefore it gets more possible to produce equiaxed grains [27].

As the superheat amount increases, the time for the metal to solidify also increases. This results in a deeper sump. However, this additional heat is not very significant compared to the latent heat released during solidification.

Figure 2.19 shows the effect of headbox level (metallostatic head) on the position of the meniscus. (a) represents low level, (b) represents optimal level, (c) represents high level. The casting speed is the same in each case, thus for a high headbox level, the casting region is filled more, whereas with a low headbox level, substantial empty spaces between the nozzle tip and the casting roll are detected.

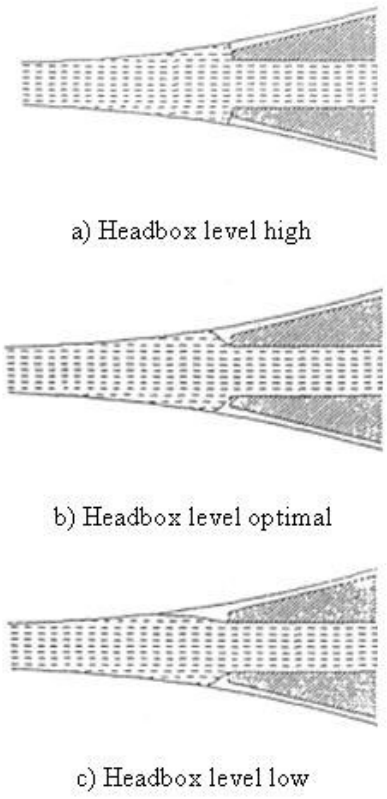

Figure 2.19. Position of the meniscus corresponding to different headbox levels [27]

In TRC, a graphite release agent is applied to the casting rolls by a traversing spray system to prevent the aluminum sheet from sticking to the roll shell. On the other hand, graphite hampers the heat transfer forming an insulation layer on the rolls. This attribute is used to the advantage of the operator: the operator can freely decide which areas of the roll surface will be sprayed by placing obstructions in front of the graphite nozzle. Areas with graphite will have low heat transfer coefficients whereas unsprayed areas will have higher heat transfer coefficients. In this way, bleed-outs can be prevented up to a point.

The cooling of the rolls is primarily done with the circulating water in the channels between the roll shell and the roll core. The flowrate of the cooling water can be freely adjusted.

2.6. Formability

Sheet metal forming is the process of converting a flat sheet of metal into a part of desired shape without fracture or excessive localized thinning. Therefore, the formability of a material can be defined as the extent to which it can be deformed in a particular process before the onset of failure. In sheet stamping, this extent is influenced by three types of variables [28]:

- Design variables (shape, curvature)
- Process variables (die alignment, hold down pressure, lubrication)
- Material variables (yield and ultimate strength, elongation)

However, in production, these variables are adjusted to attain maximum production rates at minimum cost and therefore require the utmost from the material properties. A complete evaluation requires actual press trials where all three variables come into play [28].

Formability is one of the most important properties of aluminum and its (wrought) alloys for which plastic forming is the most important step in semi production, processing and downstream applications and in-service parts behaviour [29].

Aluminum and its alloys are among the most readily formable of the commonly fabricated metals. There are, of course, differences between aluminum alloys and other metals in the amount of permissible deformation, in some aspects of tool design, and in details of procedure. These differences stem primarily from the lower tensile and yield strengths of aluminum alloys, and from their comparatively low rate of work hardening. The wide range of compositions and tempers of aluminum alloys also affects their formability [30].

Aluminum alloy sheet usually fails during forming either by localized necking or ductile fracture. Necking is governed largely by material properties such as work hardening and strain-rate hardening and depends critically on the strain path followed by the forming process. In dilute alloys, the extent of necking or limit strain is reduced by cold work, age

hardening, gross defects, large grain size, and the presence of alloying elements in solid solution. Ductile fracture occurs as a result of the nucleation and linking of microscopic voids at particles and the concentration of strain in narrow shear bands. Fracture usually occurs at larger strains than does localized necking and therefore is usually important only when necking is suppressed. Common examples where fracture is encountered are at small radius bends and at severe drawing, ironing, and stretching near notches or sheared edges [30].

Considerable advances have been made in the development of alloys with good formability, but, in general, an alloy cannot be optimized on this basis alone. The function of the formed part must also be considered, and improvements in functional characteristics, such as strength and ease of machining, often tend to reduce the formability of the alloy [30].

2.6.1. Effect of Material Properties on Formability

The properties of sheet metals vary considerably, depending on the base metal (steel, aluminum, copper, etc.), alloying elements present, processing, heat treatment, gage, and level of cold work. In selecting material for a particular application, a compromise usually must be made between the functional properties required in the part and the forming properties of the available materials. For optimum formability in a wide range of applications, the work material should [31];

- Distribute strain uniformly,
- Reach high strain levels without necking or fracturing,
- Withstand in-plane compressive stresses without wrinkling,
- Withstand in-plane shear stresses without fracturing,
- Retain part shape on removal from the die,
- Retain a smooth surface and resist surface damage.

Three material properties determine the strain distribution in a forming operation: the strain-hardening coefficient (also known as the work-hardening coefficient or exponent) or n value, the strain-rate sensitivity or m value, and the plastic strain ratio (anistropy factor)

or r value. The ability to distribute strain evenly depends on the n value and the m value. The ability to reach high overall strain levels depends on many factors, such as the base material, alloying elements, temper, n value, m value, r value, thickness, uniformity, and freedom from defects and inclusions.

The n value, or strain-hardening coefficient, is determined by the dependence of the flow (yield) stress on the level of strain. In materials with a high n value, the flow stress increases rapidly with strain. This tends to distribute further strain to regions of lower strain and flow stress. A high n value is also an indication of good formability in a stretching operation [31].

The m value, or strain-rate sensitivity, is defined by:

$$m = \frac{d \ln \sigma}{d \ln \dot{\varepsilon}} \tag{2.1}$$

where $\dot{\varepsilon}$ is the strain rate, $d\varepsilon/dt$. This implies a relationship of the form:

$$\sigma = f(\varepsilon)\, \dot{\varepsilon}^{m} \tag{2.2}$$

or

$$\sigma = k\varepsilon^{n} \dot{\varepsilon}^{m} \tag{2.3}$$

where Equation 2.3 equation incorporates

$$\sigma = k\varepsilon^{n} \tag{2.4}$$

between stress and strain.

A positive strain-rate sensitivity indicates that the flow stress increases as the rate of deformation increases. This has two consequences. Higher stresses are required to form parts at higher rates. Also, at a given forming rate, the material resists further deformation in regions that are being strained more rapidly than adjacent regions by increasing the flow stress in these regions. This helps to distribute the strain more uniformly [31].

High n and m values lead to good formability in stretching operations, but have little effect on drawability. In a drawing operation, metal in the flange must be drawn in without causing fracture in the wall. In this instance, high n and m values strengthen the wall, which is beneficial, but they also strengthen the flange and make it harder to draw in, which is detrimental [31].

The r value, or plastic strain ratio, relates to drawability and is known as the anisotropy factor. This is defined as the ratio of the true width strain to the true thickness strain in the uniform elongation region of a tensile test [31]:

$$r = \frac{\varepsilon_w}{\varepsilon_t} = \frac{\ln\left(\frac{w}{w_0}\right)}{\ln\left(\frac{t}{t_0}\right)} \tag{2.5}$$

The r value is a measure of the ability of a material to resist thinning. In drawing, material in the flange is stretched in one direction (radially) and compressed in the perpendicular direction (circumferentially). A high r value indicates a material with good drawing properties [31].

The r value frequently changes with direction in the sheet. In a cylindrical cup drawing operation, this variation leads to a cup with a wall that varies in height, which is known as earing (Figure 2.20). It is therefore common to measure the average r value, or average normal anistropy, r_m, and the planar anisotropy, Δr.

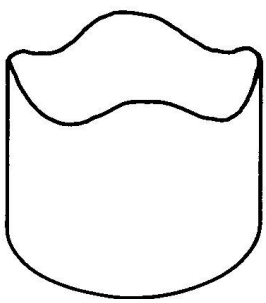

Figure 2.20. Drawn cup with ears in the directions of high r value

The property r_m is defined as

$$\frac{r_0 + 2r_{45} + r_{90}}{4} \tag{2.6}$$

where the subscripts refer to the angle between the tensile specimen axis and the rolling direction. Δr is defined as

$$\frac{r_0 - 2r_{45} + r_{90}}{2} \tag{2.7}$$

It is a measure of the variation of r with direction in the plane of a sheet, r_m determines the average depth (i.e., the wall height) of the deepest draw possible. Δr determines the extent of earing. A combination of a high r_m value and a low Δr value provides optimum drawability.

It is known that in an isotropic material

$$r_0 = r_{90} = r_{45} = 1 \tag{2.8}$$

Therefore, from Equations 2.6 and 2.7:

$$r_m = 1 \tag{2.9}$$

and

$$\Delta r = 0 \tag{2.10}$$

High r_m and a low Δr values are desired in forming operations, especially in deep-drawing. A high r_m value increases the limiting drawing ratio of the material, while a low Δr value decreases the tendency of the material to form ears during the deep-drawing operations. Ears are objectionable on drawn cups, because they have to be trimmed off, resulting in scrap [32].

Some BCC metals, such as steel, exhibit high r value (>1.8) and low Δr value (<0.4), resulting in high formability and low earing. On the other hand, FCC metals, such as Al and Cu, tend to have low r-value (<0.8) and high Δr value (~0.6) [33].

2.6.2. Types of Formability Tests

Sheet metal forming operations are so diverse in type, extent, and rate that no single test provides an accurate indication of the formability of a material in all situations. However, knowledge of material properties and careful analysis of the various types of forming involved in making a particular part are indispensable in determining the probability of successful part production and in developing the most efficient process.

Formability tests are of two basic types: intrinsic and simulative. Intrinsic tests measure the basic characteristic properties of materials that can be related to their formability. Simulative tests subject the material to deformation that closely resembles the deformation that occurs in a particular forming operation [31].

Intrinsic tests provide comprehensive information that is insensitive to the thickness and surface condition of the material. The most important and extensively used intrinsic test is the uniaxial tensile test, which provides the values of many material properties for a wide range of forming operations. Other commercially important intrinsic tests are the plane-strain tensile test, the Marciniak stretching and sheet torsion tests, the hydraulic bulge test, the Miyauchi shear test, and hardness tests [31].

Simulative tests provide limited and specific information that is usually sensitive to thickness, surface condition, lubrication, and geometry and type of tooling. For many forming operations, tests that simulate the operation are more useful and relevant than fundamental intrinsic property measurement tests. These tests subject the work material to deformation that closely approximates the production operation, including the effects of factors not present in the intrinsic tests, such as bending and unbending and friction between the work materials and die surfaces. Because these additional factors are present, simulative tests tend to be less reproducible than intrinsic tests and must be performed under carefully controlled conditions to minimize variability in the results [31].

Simulative tests can be classified on the basis of the predominant forming operation involved: bending, stretching, drawing, and stretch-drawing. For instance, ball punch tests, such as the Olsen cup test and Erichsen cup test have been used to determine the properties of sheet metals in stretching. In addition, tests have been developed to measure wrinkling and the springback that occurs after bending or another forming operation [31].

2.6.3. The Forming Limit Diagram

A significant practical departure from the traditional methods for assessing the press-shop performance of sheet metals occurred in 1965 when Keeler and Goodwin introduced the concept of forming limit diagrams (FLDs). The results of this early work implied a sensibly constant FLD relationship for a variety of annelead materials and indicated how, by changing the stress and strain conditions under the press in ways that hitherto would not always have been immediately obvious, failures could be avoided [34].

The idea behind the FLD is that each sheet metal can be deformed only to a certain level before local thinning (necking) and fracture occur. This level depends principally on the combination of strains imposed, i.e., the ratio of major and minor strains. The lowest level occurs at or near plane strain, i.e., when the minor strain is zero [30].

This information was first represented graphically as the FLD, which is a graph of the major strain at the onset of necking for all values of the minor strain that can be realized. Figure 2.21 shows a typical forming limit diagram for steel. The diagram is used in combination with strain measurements, usually obtained from circle grids, to determine how close to failure (necking) a forming operation is, or whether a particular failure is due to inferior work material or to a poor die condition [30].

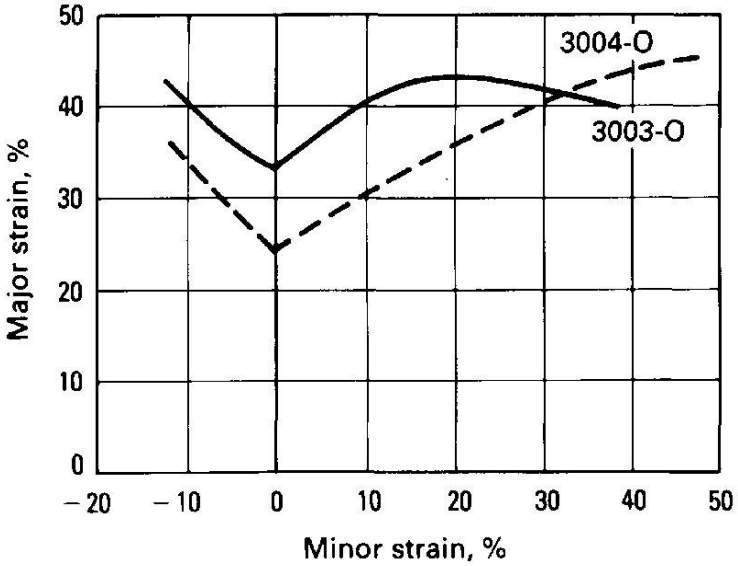

Figure 2.21. Forming-limit diagrams for two 3xxx series aluminum alloys [30]

The shape of the forming limit curve (FLC) in Figure 2.21 differs for each metal, for each alloy of a metal and even for the tempers of the alloy type. The position of the curve also varies with changes in the thickness and the orientation of the sheet, r_m and n values, and the state of prestrain. An optimum formability appears in thicker sheets with high n, low r_m, a 45º orientation and compressive prestrain [35]. The intercept of the curve with the vertical axis represents plane strain and is also the minimum point on the curve.

The forming limit diagram is also dependent on the strain path. The standard diagram is based on an approximately uniform strain path. Diagrams generated by uniaxial straining followed by biaxial straining, or the reverse, differ considerably from the standard diagram. For this reason, the effect of the strain path must be taken into account when using the diagram to analyze a forming problem [30].

FLD's are beneficial in many ways for the sheet metal forming industry. For instance, Figure 2.22 illustrates the FLD of low-carbon steel and gives the permissable deformations at various strain ratios. Point A in this diagram is a critical point and indicates the failure of the specimen between plane strain and balanced biaxial strain. Several remedies, some of them not intuitively evident, may then be explored to bring strains within allowable limits:

- Increase the minor strain by clamping more firmly in that direction.
- If fracture occurred away from the apex, improve lubrication to redistribute strains.
- If all else fails, the part will have to be redesigned to reduce the major strain, or some material must be allowed to flow into the die, changing the process into combined stretch-drawing [32].

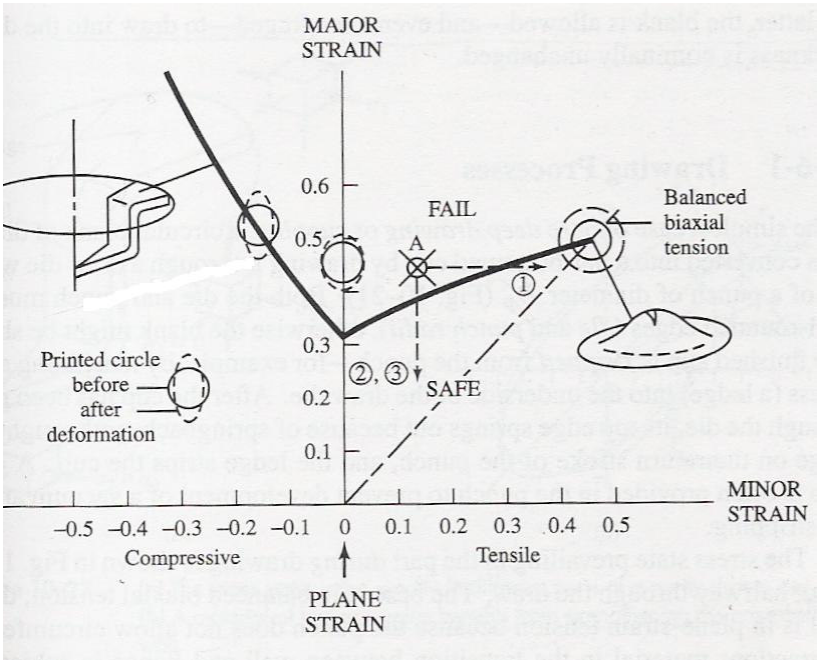

Figure 2.22. The forming limit diagram typical of low-carbon steel gives the permissible deformations at various strain ratios [32]

3. EXPERIMENTAL STUDY

Uniaxial tension tests and Erichsen tests were conducted to investigate the formability properties of the AA1050 sheet metal, twin-roll cast at different solidification parameters. In addition, dome stretch tests were performed to predict the forming limit diagram of the AA1050 sheet metal. A microhardness study was also conducted to determine the hardness values of the specimens cast at different solidification parameters. The typical nominal composition of AA1050 is shown in Table 3.1.

Table 3.1. The typical nominal composition of AA1050 [36]

Al	Si	Fe	Cu	Mn	Mg	Cr	Ni	Zn	Ti	Ga	V	Others
99.50	0.25	0.40	0.05	0.05	0.05	--	--	0.05	0.03	--	0.05	0.03

3.1. Preparation of the Specimens

The sheet metal blanks for the experimental study were obtained from the commercial twin-roll casting lines of Assan Alüminyum A.Ş. As shown in Table 3.2, 6 groups of samples were prepared. Samples of the groups 1-2 were cast at the same casting gauge and roll diameters. They only differed in the casting speed. Thus, groups 1-2 were aimed at finding the effect of casting speed on the formability behaviour of aluminum sheet. Similarly, groups 3-4 differed in the roll diameter and groups 5-6 differed in the casting gauge.

Table 3.2. 6 groups of samples cast under different solidification conditions

Group No / **Solidification Parameter**	**1**	**2**	**3**	**4**	**5**	**6**
Casting Gauge	3.0 mm	3.0 mm	5.0 mm	5.0 mm	5.5 mm	5.0 mm
Casting Speed	2.50 m/min	2.75 m/min	1.70 m/min	1.70 m/min	1.50 m/min	1.50 m/min
Roll Diameter	1000 mm	1000 mm	600 mm	1000 mm	1000 mm	1000 mm

As illustrated in Table 3.2, the objective of the current work is to study the effects of three significant solidification parameters, namely the casting speed, the casting gauge and the roll diameter, on the formability behaviour of the twin-roll cast AA1050 strip. As mentioned in Section 2.5.4. “Solidification Parameters”, there are also other important casting parameters such as the the superheat of the molten metal and the tip-setback, which influence the formability of the sheet metal. However, these parameters were not included in the experimental study due to two reasons:

The casting lines at Assan Alüminyum A.Ş. are industrial casting lines which operate 24 hours a day. Once the casting process reaches the steady state, changing of these parameters is risky in terms of the continuity of the casting. For instance, a slight drop in the superheat amount may cause the metal to solidify in the tip and may cause the termination of the casting process. On the other hand, a slight increase may cause the sheet metal to leave the casting rolls partially molten. In addition, since these are dependent parameters, they can not be freely altered while holding other parameters constant. For instance, the superheat amount can only be changed if the casting speed or the casting gauge is also changed.

Because the as-cast sheet of 3 mm and 5 mm could not be directly used in most formability testing methods, all samples were initially cold rolled to 1.5 mm and annealed to 0-condition.

Cold rolling was done at an experimental cold rolling machine of the Quality System Laboratory (QSL) of Assan Alüminyum A.Ş. 5mm thick sheets were cold rolled to 1.5 mm in two steps. First step from 5 mm to 2.7 mm; second step from 2.7 mm to 1,5 mm. 3 mm thick sheets were cold rolled to 1.5 mm in a single pass. The annealing processes were done in the Nabertherm Anneling furnaces of the QSL of Assan Alüminyum A.Ş. The residence time of the samples at 410°C was 4 hours; and the total residence time in the furnace was 7 hours.

Figure 3.1 briefly illustrates the experimental procedure followed in the current work.

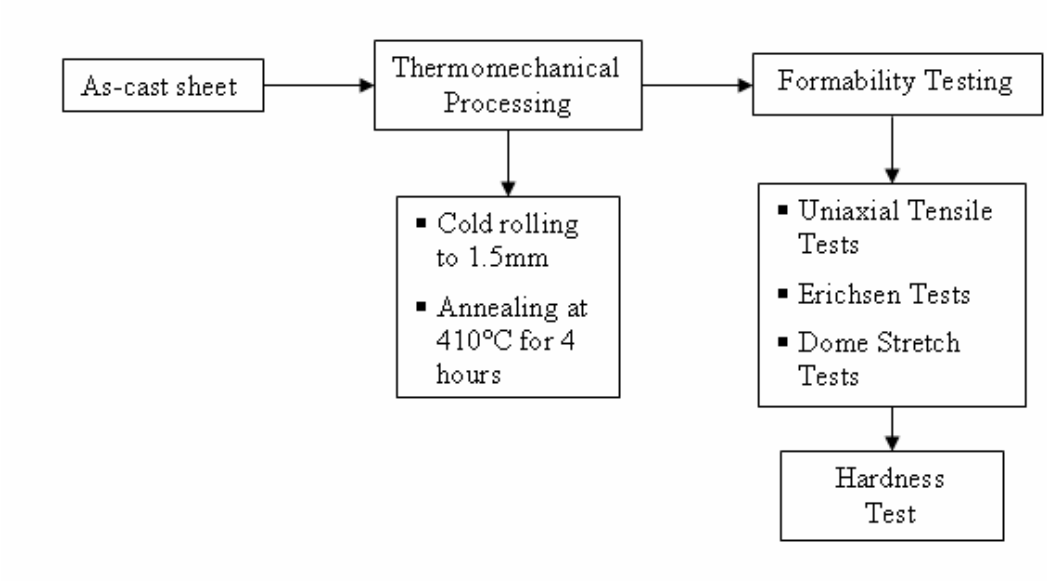

Figure 3.1. The experimental procedure followed in the current work

Various blanks from the 1.5mm thick, 0-condition AA1050 sheet were prepared at different sizes for the mechanical tests:

The uniaxial tensile test specimens were prepared according to ASTM Standard E-8 [37] at 0º, 45º and 90 ºC orientations to the rolling direction. Erichsen test specimens were prepared in sizes of 70x300 mm. For the dome stretch tests, three different specimen types were prepared to simulate different strain conditions: 110x110 mm for biaxial strain, 110x50 mm for plane strain and 110x75 mm for between the area of plane strain and balanced biaxial strain. Each specimen had their long sides parallel to the rolling direction. For the microhardness tests, specimens were cut from transverse cross-sections and cold mounted in bakelite.

Both the dome stretch specimens and the uniaxial tensile testing specimens were electrochemically etched before the mechanical tests for the prediction of the FLD's.

3.1.1. Electrochemical Etching

The electrochemical etching process was performed at the QSL of Assan Alüminyum A.Ş. In order to determine the FLC's for different parameter groups, grids of 2.5 mm

circles were marked on the sheets with the electrochemical etching method. The etching device is illustrated in Figure 3.2. The following steps were involved in marking the grid by this method:

- Cleaning the surface of the blank with ethyl alcohol to remove any dirt or lubricating oil from the previous cold rolling step (This cleaning step was performed before the annealing of the samples).

- Placing the stencil on the blank to be etched (The stencil is a plastic sheet which holds the pattern of circular grids as gaps).

- Placing the pad soaked with the electrolyte on the stencil (The constituents of the electrolyte is listed in Table 3.3).

- Switching on the power supply and setting the voltage (The current drawn is dependent on the applied pressure and the stencil size)

- Rolling the electrode on the felt pad and applying pressure. After applying pressure with the electrode, the felt pad will squeeze, the electrolyte will pass through stencil and come in contact with the blank, etching the grid pattern electrochemically into the blank.

- Finally rinsing the electrode with water to prevent oxidation.

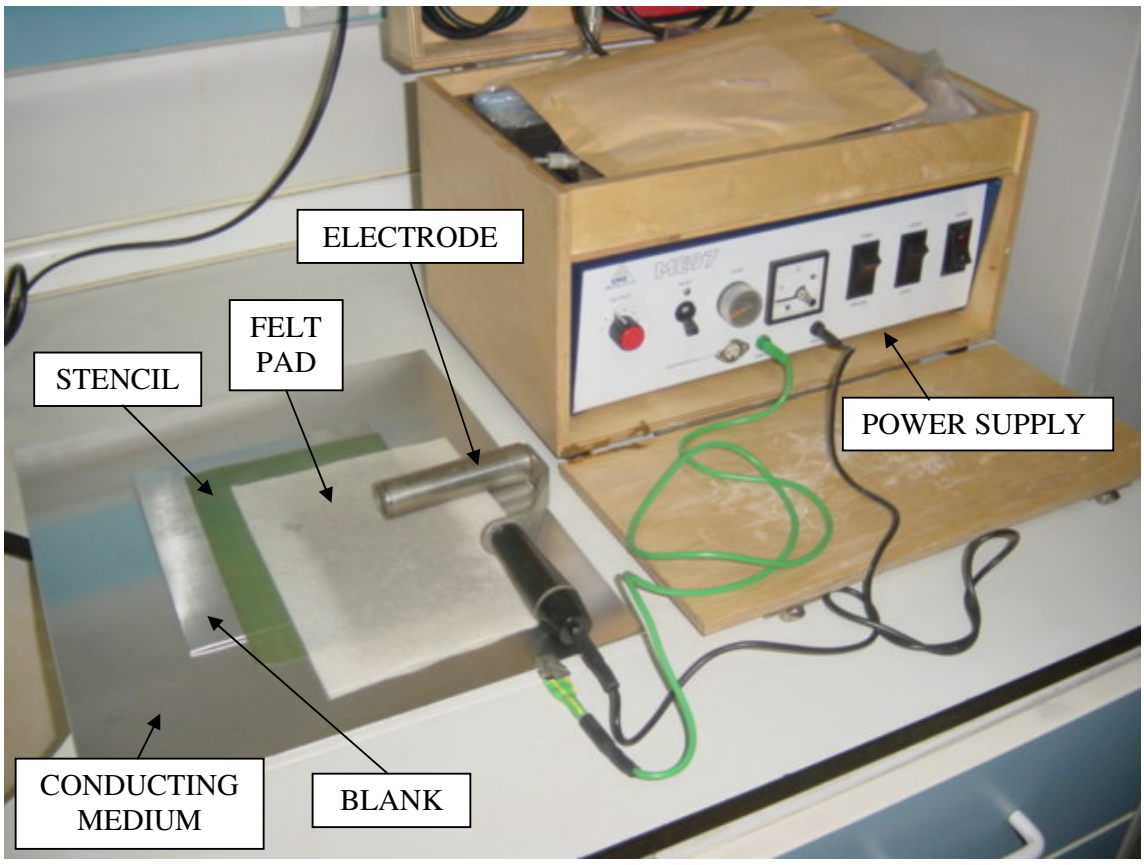

Figure 3.2. The electrochemical etching device and prepared setup

Table 3.3. The constituents of the electrolyte used in the etching process

Potassium chloride	80 g
Sodium chloride	90 g
Nitric acid	100 ml
Hydrochloric acid	100 ml
Water	4.5 l

Further information about the procedure and the details of the etching process can be obtained from ASTM E2218-02 [38].

3.1.2. Grid Strain Analysis

To measure the strains from the deformed circular grids, initially a photo of the undeformed specimen (Figure 3.3) was taken under an Olympus SZ-ET stereomicroscope

at 2x magnification. Afterwards, the image was transferred to a PC software to measure the undeformed length in pixels. Since the dimensions of the undeformed grid is known in both pixels and millimeters (2.5 mm in the current work) beforehand, it is simple direct proportion switching between pixels and millimeters while calculating the strain values for the deformed dome stretch test specimens (Figure 3.4)

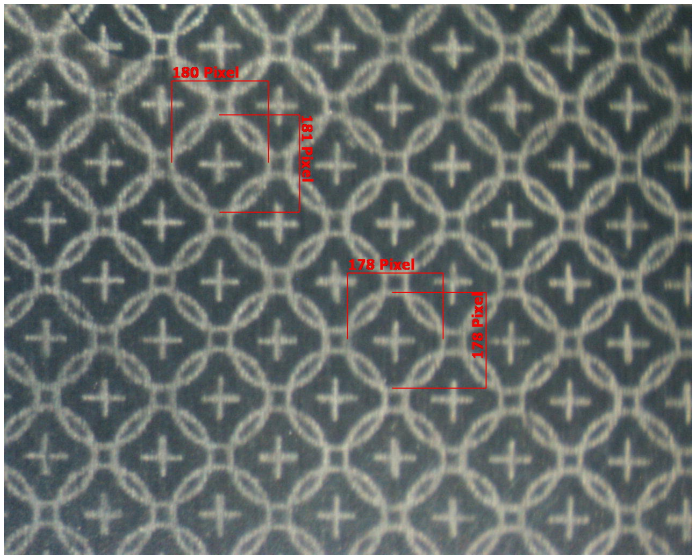

Figure 3.3. A photo the undeformed and etched specimen

The strains from the deformed specimens were calculated as follows:

After the deformation process, the selected critical areas (see Section 3.2.3 “Dome Stretch Test” for the selection of critical areas) were measured for the resulting gage length changes in the long dimension from (l_o) to (l_f) of the pattern, and in the width dimension (w_o) to (w_f) at 90° to the long dimension as shown in Figure 3.4. The major strain (e_1) and associated minor strain (e_2) at 90° to (e_1) were calculated from these gage length changes. The strains were calculated as engineering strain in percent based on the original gage length according to Equation 3.1 [38].

$$e_1 = \frac{l_f - l_o}{l_o} * 100 \tag{3.1}$$

By convention, major strain (e_1) is measured along the major axis of the ellipse resulting from deformation of a circular grid pattern. On the other hand, the minor strain (e_2) is the strain in the sheet surface in a direction perpendicular to the major strain [38].

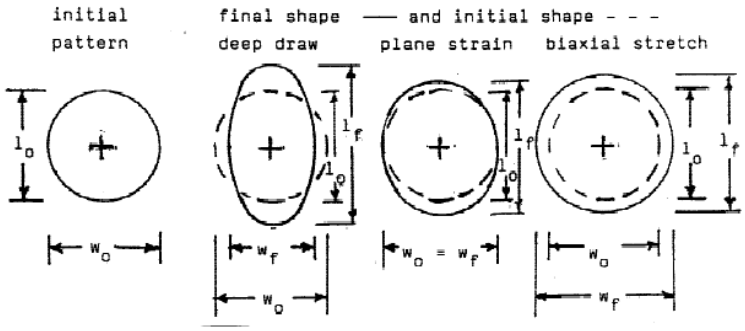

Figure 3.4. Possible changes in shape of the grid pattern caused by forming operations on metallic sheet products [38]

For the dome stretch tests, since the grids being measured are on a curved surface, there is an inevitable, small amount of error in the calculations. To get the exact strain value, one has to measure the arc length on the curved surface, but with the current method it is only possible to measure the projection of the arclength from the images (Figure 3.5). This error is neglected in the calculations.

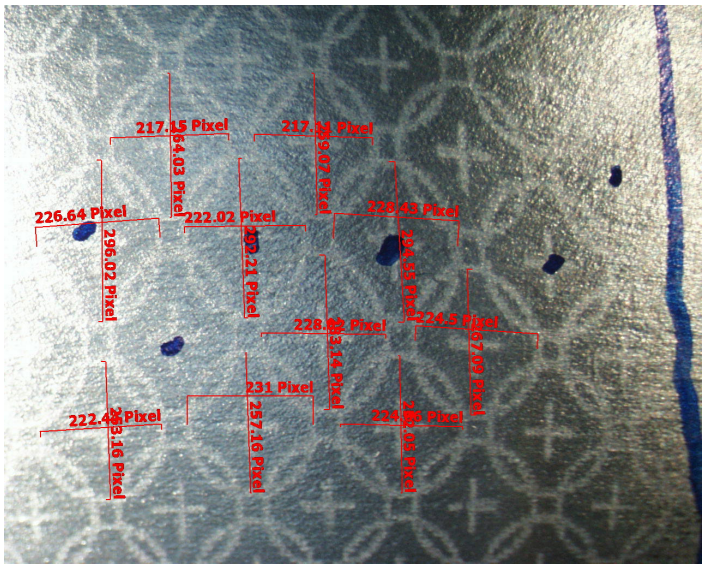

Figure 3.5. A photo the deformed and etched specimen

3.2. Mechanical Tests

3.2.1. Uniaxial Tensile Test

Uniaxial tensile test is the most widely used intrinsic formability testing method in the sheet metal forming industry. Basically, a “dog bone” shaped specimen is gripped at each end and stretched at a constant rate in a tensile machine until it fractures, as described in ASTM Standard E8, "Methods of Tension Testing of Metallic Materials" [37]. The applied load and extension are measured by means of a load cell and strain gage extensometer.

Uniaxial tensile tests were done to determine the basic mechanical properties like the yield strength and tensile strength, strain-hardening coefficient (n) and the anisotropy factor or the plastic strain ratio (r) of the AA1050 sheet metal. Electrochemically etched uniaxial tensile test specimens were also utilized in the characterization of the FLD’s (Figure 3.6).

Figure 3.6. Electrochemically etched uniaxial tensile test specimens

Tests were performed at a Zwick testing machine with a 50 kN load cell at the QSL of Assan Alüminyum A.Ş. A constant strain rate of 10 mm/min was applied. Testing was done at room temperature and extensions were measured using a 50.8 mm extensometer.

TestXpert, the commercial sofware package of the Zwick testing machine, was utilized for the calculation of the above mentioned mechanical properties.

For the calculation of the strain-hardening coefficient n of the empirical hardening law, Equation 2.4. was expressed in the logarithmic form in terms of true stress and true strain:

$$\log \sigma = \log k + n \log \varepsilon \tag{3.2}$$

The values of true stress and true strain were calculated from the following equations:

$$\sigma = S(1+e) \tag{3.3}$$

$$\varepsilon = \ln(1+e) \tag{3.4}$$

where (σ, ε) is a true stress versus true strain pair in the selected interval, S is the engineering stress and e is the engineering strain.

The n value was calculated by the TestXpert software within the 5% and 10% plastic strain range via linear regression analysis of $\log \sigma$ and $\log \varepsilon$ with 5 data pairs selected within this range.

For the calculation of the r-value, a width extensometer was attached to the tensile testing machine to continuously measure the width change throughout the test. From these values, the r-value was determined according to ASTM Standard E 517-81 “Plastic Strain Ratio r for Sheet Metal” [39] from Equation 3.5.

$$r = \frac{\ln\left(w_o / w_f \right)}{\ln\left(l_f w_f / l_o w_o \right)} \tag{3.5}$$

where w_o, w_f, l_o and l_f denote the original width, final width, original length and final length of the tensile test specimen, respectively.

As mentioned in Section 3.1 "Preparation of Samples", tensile test specimens were prepared at 0º, 45º and 90 ºC orientations to the rolling direction. This is due to the fact that during the rolling process used to produce metals in sheet form and subsequent annealing, the grains and any inclusions present become elongated in the rolling direction, and a preferred crystallographic orientation develops. This causes a variation of properties with direction. Thus, it is common practice to test specimens cut parallel to the rolling direction and at 45° and 90° to this direction. These are known as longitudinal, diagonal, and transverse specimens, respectively. This also enables the values of r_m and Δr to be calculated. While r_m is a measure of normal anisotropy, Δr value gives information about the planar anisotropy of a material. Because the mechanical properties and elongation tend to be lower in the transverse direction, tests in this direction are often used as the basis for specifications.

Average r value, r_m and planar anisotropy value, Δr were calculated according to Equations 2.6 and 2.7.

The r-values were calculated at 3 predefined points of 9%, 10% and 11% plastic strain significant to 0.01 as indicated in ASTM E 517 [39].

3.2.2. Erichsen Test

Tests were performed on a manual Erichsen testing machine at the QSL of Assan Alüminyum A.Ş. The machine had a punch diameter of 10mm. Specimens were lubricated with oiled polyethylene. The forward movement of the punch was stopped at the fracture of the specimen and the height at fracture was used as the measure of stretchability.

Figure 3.7 shows the Erichsen test specimen. 3 readings were taken from each specimen and 2 specimens were used for each parameter group. The measured values are significant to 0.1 mm.

Figure 3.7. Erichsen Test Specimen

3.2.3. Dome Stretch Test

Dome stretch tests were performed to determine the FLD's and the limiting dome height (LDH) values for the 0-condition, 1.5 mm AA1050 sheet metal. Tests were performed at the Instron 1186 testing machine in the materials laboratory of Boğaziçi University. Samples were lubricated with a commercial type grease. The die and the punch used for stretching the samples are illustrated in Figure 3.8. The tensile testing machine had a load cell with a range of 100 kN. The punch had a constant velocity of 5 mm/min.

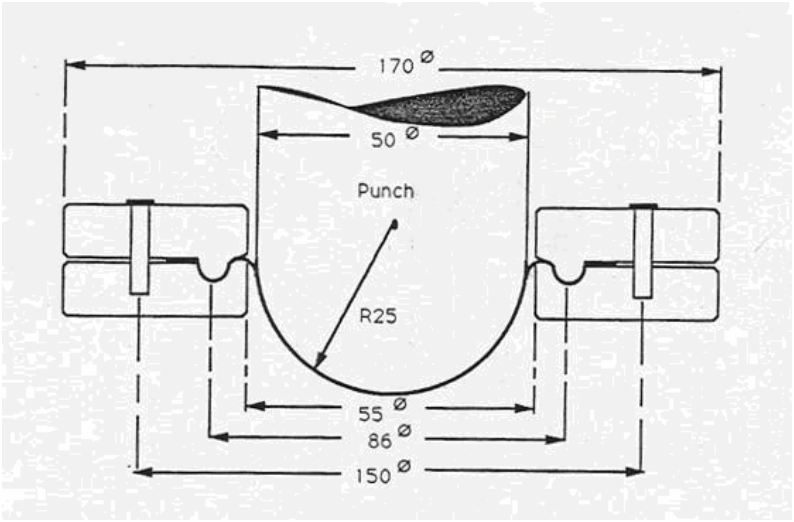

Figure 3.8. The geometry of the dome stretch test device [28]

Dome stretch test was designed to give a repeatable measure of punch movement among specimens of a specific sheet sample, thus the only measured value would be the punch height at incipient fracture. While problems with maintaining a secure clamping of the specimen result in variation of the measured LDH value, they are not critical for the determination of the FLC [38].

The height at which the specimen failed was monitored along with the force being exerted on the specimen by the punch of the stretch test device. The maximum height achieved (LDH) was the height at which the force dropped off, which implied a localized necking on the specimen. At this maximum height, the punch advance was stopped manually as quickly as possible (Figure 3.9).

As seen in Figure 3.9, there is a short period where there is no force applied on the punch. At this moment, the punch is not in contact with the specimen. As soon as the punch comes into contact and starts deforming the specimen, the force values start to increase. Knowing the velocity of the punch and the time elapsed while the punch is in contact with the specimen, LDH was calculated.

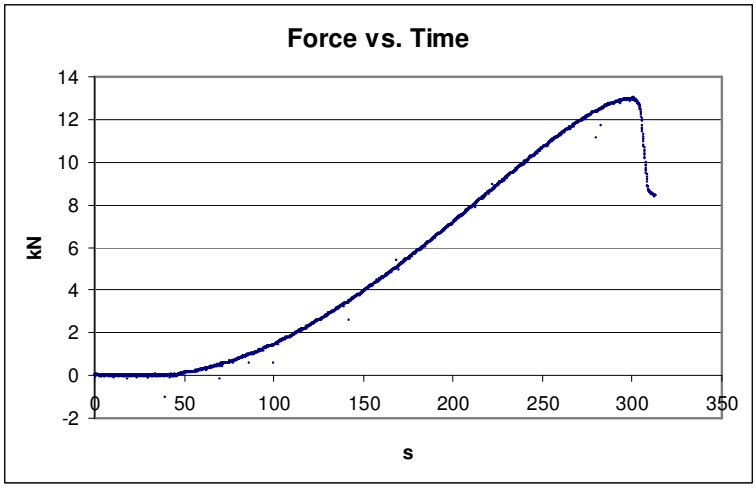

Figure 3.9. Force vs time plot for the dome stretch test

As mentioned in Section 3.1 “Preparation of Samples”, three different sample sizes were used to simulate different strain states: 110x110 mm for biaxial strain (like the strain

obtained when blowing a spherical baloon), 110x50 mm for plane strain and 110x75 mm for the strain conditions between biaxial strain and plain strain (Figure 3.10).

Figure 3.10. Three types of specimens used in the dome stretch test. (a) 110x110 mm, (b) 110x75 mm and (c) 110x50 mm

A fourth sample type with dimensions of 110x30 mm was used to simulate the uniaxial strain (simple tension). However due to the metal being very soft, there was thinning in the draw-bead regions of the die, where the clamping forces were applied. When the sample was stretched in this position, it failed from this thin region without any significant stretching in the centre region. Thus, instead of the dome stretch test specimens, fractured uniaxial tensile test specimens were used in the characterization of the FLD for the simulation of uniaxial strain. In addition, LDH values could only be obtained for the 110x110 mm and 110x75 mm specimens, because 110x50mm specimens easily deformed and lost their flatness under the locking force of the die-beads, making the calculation of the LDH impossible.

All specimens were prepared with their long dimensions parallel to the rolling direction. The distance between FLD percentage increments were same for both the major strain (e_1) ordinate (parallel to the vertical y axis) and minor strain (e_2) abscissa (parallel to the horizontal x axis) [38].

After the stretching of the specimens, minor and major strains were measured from the circular grid pattern near the necked, or fracture, location. These data points were identified in determining the FLC. The measurements included good (no localized necking), marginal (localized necking), and fracture areas. In the current work, areas with no localized necking were considered as acceptable, whereas both marginal and fracture

areas were considered together, as unacceptable. The FLC's were established by connecting the uppermost good major strains over the associated minor strain range. The formation of the FLC was partly based on judgement: There were occasionally good points above the FLC and marginal points below the FLC.

3.2.4. Brinell Hardness Test

Brinell hardness tests were performed for each parameter group at the QSL of Assan Alüminyum A.Ş. Specimens were cut from 0-condition, 1,5mm, AA1050 sheets parallel to the rolling direction and cold mounted in bakelite. The specimens were also finished with colloidal silica and etched with Barker's reagent for further microstructural characterization. 5 readings were taken for each of the 6 parameter group from the middle of the sections. A weight of 2 kg was applied for 5 seconds and dimensions of the indentation were measured with a low-power microscope. The resulting Brinell Hardness value was calculated according to Equation 3.6.

$$HB = \frac{2P}{\pi D\left(D - \sqrt{D^2 - d^2}\right)} \tag{3.6}$$

where P is load in kg; D is ball diameter in mm; and d is diameter of the indentation in mm.

3.3. Microstructural Study

It has long been known that the anisotropy of the mechanical properties and the formability of metals classically used in sheet forming, such as aluminum alloys and low carbon steels, depend on their crystallographic texture and grain size. More generally, it can be said that all microstructural features affect the plastic response of the material; apart from the above mentioned ones, these include the state of work hardening, the dislocation arrangement, the grain shape [40].

The microstructural study in the current work was limited with the investigation of the grain size and segregation behaviour of the 0-condition, AA1050 sheet metal cast at

different solidification parameters. Since the microstructure of the as-cast strip is sensitive for twin-roll casting conditions and it will greatly influence the mechanical properties not only on as-cast strip but also on annealed strip [2], the micrographs of the as-cast strips were also included. The verification of the famous Hall-Petch relationship between macroscopic stress and grain size (the smaller the grain size, the higher the stress and the lower the formability) was investigated. No work was conducted about the effects of crystallographic texture on the formability behaviour.

3.3.1. Preparation of the Specimens

As discussed previously in Section 3.2.4, specimens were sectioned from 0-condition, 1.5 mm, AA1050 sheets parallel to the rolling direction and cold mounted in bakelite. The specimens were also finished with colloidal silica and etched with Barker's reagent. Optical microscope was utilized for the examination of the microstructures.

3.4. Prototype Twin-Roll Caster

Within the scope of the current work, the existing hot rolling machine in the Materials Laboratory was revised into a twin-roll caster. Using the existing motor, transmission, locking system and chassis of the hot rolling machine, the rolls and bearings were replaced, and new housings were manufactured. Rotary joints were assembled to the rolls to facilitate water cooling within the cylinders. A metal delivery system was developed to feed the molten metal from crucible to the rolls.

3.4.1. Construction

The technical drawings related to the construction of the prototype twin-roll caster can be found in the Appendix.

The rolls comprised of two parts: the shell and the core. The shell was a hollow cylinder with an inner diameter of 160mm and an outer diameter of 200 mm. Its length was 250 mm. The shell, after being heated at 250ºC for about 1 hour, was shrink fitted to the core, which was machined to a diameter of 160+0.4 mm and fastened with the flanges. The

core had grooves on the surface as a passage for the cooling water. With the use of the rotary joints, the cooling water enters the rolls, circulates the spiral grooves and leaves the rolls from the same side. For the prototype twin-roll caster built within the scope of the current work, shells and cores were manufactured from AISI 1040 carbon steel billets by turning on a Universal Lathe. The hardness of the shells was 40 HRC.

In the conventional rolling process, the roll separating forces are approximately calculated using the formula

$$F = \left(\frac{\bar{p}}{\bar{\sigma}_{av}} \right) \bar{\sigma}_{av} \, A_x \tag{3.7}$$

Basically, separating force is equal to the product of the contact area between the rolled material and the roll pass, A_x the mean unit pressure, $\bar{p}$ on the roll and the average flow stress, $\bar{\sigma}_{av}$ within the roll gap. However, for TRC, there is not an established formula for the calculation of the roll separating forces in the literature. The separating forces are directly dependent on the solidification mechanism in the casting region, i.e. the position of the solidification front, the temperature and the type of the alloy being cast, casting speed, etc. From the cast-shop experiences of Assan Alüminyum A.Ş., it was seen that for a specific alloy at a specific temperature, the separating forces change only with the casting gauge and casting width. The roll diameter has no significant effect on the separating forces. In this manner, separating forces for the prototype caster's 250 mm long rolls were calculated from simple direct proportioning. It was known that, a twin-roll caster with 2000 mm wide rolls generated about 1200 tons of separating forces at a casting gauge of 5 mm. Thus, the prototype model had to withstand approximately 150 tons.

Single housing would thus be carrying 75 tons of force. The bearings for this amount of force were selected from SKF. Spherical roller bearings were selected to resist any possible horizontal forces.

Rotary unions are devices which can be connected to rotating machineries (e.g. rotating shafts) and allow leak proof transfer of liquids from stationary sources (e.g. a supply pipe)

A typical rotating union features:

- Ball bearings to support the rotating component (attached to the machinery) against the stationary component (attached to the stationary supply source)
- Mechanical seal to seal the media passing through the rotating union

Mechanical seal face materials and secondary seals will vary depending upon the fluid properties and operating conditions of the application. Likewise, bearing type, design, material and construction will also vary with application [41]. In the prototype twin-roll caster, two rotary unions were used. Cooling water entering from one end of the union enters the shaft and circulates the rolls in the spiral grooves (Figure 3.11).

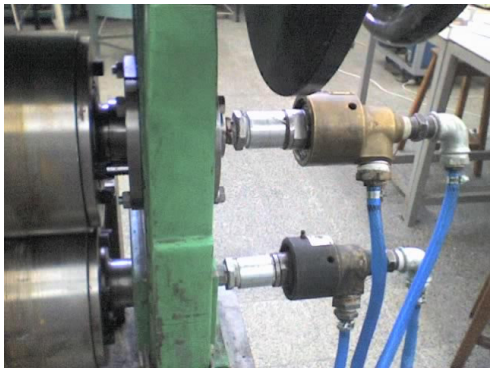

Figure 3.11. Rotary unions used in the prototype twin-roll caster

For the delivery of the molten metal to the casting rolls, a 50 mm wide feed tip was manufactured. The commercial feed tip material, which mainly consisted of SiO_2 and Al_2O_3 was used. The feeding of the liquid metal was performed manually by pouring from a melting crucible directly into inlet of the tip (Figure 3.12). The crucible used was a A-10 type, graphite crucible. The melting of the aluminum was realized in the annealing furnace of the Materials Laboratory.

Figure 3.12. Metal delivery system and the casting rolls

3.4.2. Trials

A total of 10 casting trials were completed with the prototype twin-roll caster. Different melt temperature ranges (675ºC-700ºC) and casting gauges (1.5 mm-4 mm) were tested. However, it was not possible to obtain a continuous, fully solidified and hot rolled sheet metal in any of the trials. Either the sheet left the rolls partially solidified and hot rolled (Figure 3.13), or without any solidification, at all.

Figure 3.13. As-cast, 1.5 mm strip cast with the prototype twin-roll caster

This problem possibly developed due to two issues:

- Manual feeding of the metal to the inlet of the feed tip obviously caused fluctuations in the metal amount fed to the roll bite. This resulted in discontinuous sheet production.

- Current speed of the rolls is 20 rpm. Possibly, lower speeds are required for the liquid metal to fully solidify and be hot rolled.

These two issues can be solved by:

- Implementation of a more sophisticated metal delivery system which can provide continuous metal delivery with the regulation of the metallostatic head can solve this problem.

- Replacing the current 1/46 reduction unit with one which will provide more speed reduction.

Microstructural study was conducted for the AA1050 cast strip obtained from the prototype twin-roll caster. Details can be found in Section 4.5.1 “Prototype Twin-Roll Caster Samples”.

4. RESULTS AND DISCUSSIONS

Results and discussions of the previously described mechanical tests and the microstructural study are presented in this section.

4.1. Uniaxial Tensile Test

Tables 4.1-4.6 show the uniaxial tensile test results for each of the 6 parameter groups. For each group, 6 specimens were tested: 2 specimens at 0º (numbers 1-2), 2 specimens at 45º (numbers 3-4) and 2 specimens 90º (numbers 5-6) to the rolling direction. All specimens have thickness values of $1.5 + 0.05$ mm.

Since aluminum alloys do not have a well defined yield point, yield strength is calculated at 0.2% strain. Total elongation corresponds to the total amount of strain at fracture and uniform elongation is the strain value at localized necking. As previously mentioned, r-values were calculated at 3 predefined points of 9%, 10% and 11% plastic strain and average values are listed in Tables 4.1-4.6.

Table 4.1. Mechanical Properties for the 1st Parameter Group.

	Orientation	Yield Strength at %0,2	Tensile Strength	Total Elongation	Uniform Elongation	n-val.	r-val.
Nr	mm	N/mm²	N/mm²	%	%		
1	0°	39.9	79.9	31.9	23.7	0.19	1.58
2	0°	40.9	79.9	34.0	24.2	0.18	1.48
3	45°	40.6	82.0	37.6	28.8	0.20	1.09
4	45°	37.6	82.2	39.1	29.4	0.21	0.42
5	90°	39.4	77.5	31.8	24.4	0.18	0.71
6	90°	39.0	77.9	32.1	24.6	0.18	0.76

R-values at each specimen orientation were averaged to get the values of r_0, r_{45} and r_{90}. Mean r value, r_m, and planar anisotropy value, Δr values were calculated as in Equations 2.6 and 2.7. For the 1st parameter group specimens, r_m and Δr values were found to be 0.94 and 0.38, respectively.

Since n values also show differences with different orientations, an average n-value, $\bar{n}$ is determined in a similar fashion to the r_m value:

$$\bar{n} = \frac{n_0 + 2 * n_{45} + n_{90}}{4} \tag{4.1}$$

and found as 0.19.

Likewise, the values of $\bar{n}$ and r_m were calculated for the different parameter groups. The results are listed in Table 4.7.

Table 4.2. Mechanical Properties for the 2nd Parameter Group.

	Orientation	Yield Strength at %0,2	Tensile Strength	Total Elongation	Uniform Elongation	n-val.	r-val.
Nr	mm	N/mm²	N/mm²	%	%		
1	0°	44.5	81.9	26.0	21.6	0.18	0.86
2	0°	37.8	80.7	32.0	23.4	0.19	1.25
3	45°	39.2	82.7	39.4	29.0	0.21	1.40
4	45°	36.8	82.6	39.9	28.7	0.20	1.33
5	90°	40.2	79.7	33.5	24.6	0.19	1.62
6	90°	39.9	76.6	31.2	24.0	0.18	0.79

Table 4.3. Mechanical Properties for the 3rd Parameter Group.

	Orientation	Yield Strength at %0,2	Tensile Strength	Total Elongation	Uniform Elongation	n-val.	r-val.
Nr	mm	N/mm²	N/mm²	%	%		
1	0°	39.8	84.3	42.6	26.2	0.22	0.78
2	0°	39.6	83.7	45.0	29.3	0.21	0.80
3	45°	40.3	83.6	44.1	28.6	0.21	0.81
4	45°	40.3	84.7	45.5	29.3	0.22	0.59
5	90°	39.8	83.2	43.5	27.7	0.21	0.91
6	90°	39.7	83.2	44.2	29.9	0.21	0.65

Table 4.4. Mechanical Properties for the 4th Parameter Group.

	Orientation	Yield Strength at %0,2	Tensile Strength	Total Elongation	Uniform Elongation	n-val.	r-val.
Nr	mm	N/mm²	N/mm²	%	%		
1	0°	38.4	77.6	40.1	27.0	0.21	0.73
2	0°	37.0	75.9	39.8	27.6	0.21	0.71
3	45°	37.9	78.3	45.3	30.5	0.21	0.49
4	45°	39.2	78.1	42.1	28.7	0.21	1.43
5	90°	39.0	80.9	41.3	28.5	0.21	0.66
6	90°	39.7	80.9	38.5	27.3	0.20	1.34

Table 4.5. Mechanical Properties for the 5th Parameter Group

	Orientation	Yield Strength at %0,2	Tensile Strength	Total Elongation	Uniform Elongation	n-val.	r transv.
Nr	mm	N/mm²	N/mm²	%	%		
1	0°	40.7	82.5	41.4	27.0	0.21	2.39
2	0°	40.0	84.1	48.5	28.4	0.21	0.72
3	45°	40.4	82.0	42.4	29.7	0.21	0.73
4	45°	40.3	82.3	42.5	28.4	0.21	0.41
5	90°	40.9	83.0	42.0	28.9	0.21	0.85
6	90°	41.2	82.8	44.0	28.2	0.21	0.98

Table 4.6. Mechanical Properties for the 6th Parameter Group

	Orientation	Yield Strength at %0,2	Tensile Strength	Total Elongation	Uniform Elongation	n-val.	r-val.
Nr	mm	N/mm²	N/mm²	%	%		
1	0°	40.7	82.0	37.8	26.4	0.20	0.86
2	0°	41.0	83.2	48.0	26.8	0.20	0.84
3	45°	41.9	83.4	40.0	28.2	0.20	0.60
4	45°	41.1	83.2	40.5	28.2	0.20	0.56
5	90°	40.9	80.1	38.7	27.6	0.19	0.60
6	90°	40.9	80.4	39.2	25.4	0.19	0.64

Table 4.7. $\bar{n}$ and r_m values for each parameter group

Group No	$\bar{n}$	r_m	Δr
1	0.19	0.94	0.38
2	0.20	1.25	-0.24
3	0.21	0.74	-0.10
4	0.21	0.91	-0.10
5	0.21	0.90	0.66
6	0.20	0.66	0.16

Figure 4.1 is the graphical representation of the results in Table 1.7. Values of $\bar{n}$, r_m and Δr for each parameter group are shown.

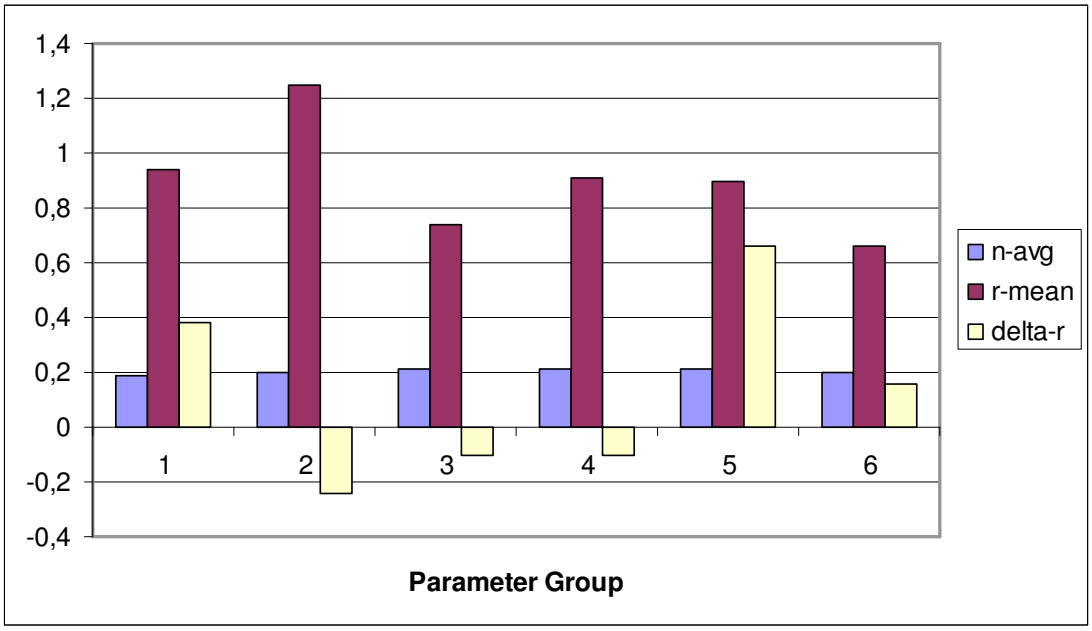

Figure 4.1. Graphical representation of the $\bar{n}$, r_m and Δr values for each parameter group.

An analysis of Figure 4.1 reveals that there is not any significant difference between the $\bar{n}$ values of different parameter groups.

In terms of the uniform elongation values, groups 1-2 have similar values averaging 25.5% and groups 3-4 have also similar values at approximately 28.4%. However, group 5

specimens have an average uniform elongation value of 28,4%, while group 6 specimens are at 27.1%.

When the Δr values are compared, it is seen that parameter group 2 specimens have Δr values closer to 0 as compared to parameter group 1 specimens (The negative value of Δr indicates earing on the 45° orientation of the sheet during the deep drawing process). Both groups 3 and 4 have very close negative Δr values. Group 5 specimens have much higher Δr values as compared to group 6 specimens, showing poor formability behaviour.

Noting that an isotropic material has an r_m value of 1, it can be concluded that specimens of parameter groups 1,4 and 5 are more isotropic than specimens of groups 2,3 and 6, respectively.

4.2. Erichsen Test

Table 4.8 shows the results of the Erichsen test performed for each parameter group.

Table 4.8. Erichsen test results for each parameter group.

Sample No / Group No	1	2	3	4	5	6	AVG
1	12.1	12.0	11.9	12.0	12.0	11.9	12.0
2	11.8	12.0	11.8	11.8	11.8	11.9	11.9
3	12.3	12.3	12.4	12.3	12.2	12.3	12.3
4	12.1	11.9	11.9	12.1	12.0	12.0	12.0
5	11.8	12.1	12.0	11.9	12.0	11.9	12.0
6	11.9	11.9	12.0	11.8	12.0	11.9	11.9

According to the results of the Erichsen test, the values of different parameter group specimens are similar. The average values range between 11.9 mm and 12.3 mm. However, if the difference of 0.3mm can be considered as significant, it can be said that the parameter group 3 specimens have better stretchability compared to group 4.

4.3. Brinell Hardness Test

Table 4.9 shows the results of the Brinell hardness test performed for each parameter group. Readings were taken from the midsections of the specimens.

Table 4.9. Brinell hardness test results for each parameter group.

Reading No / Group No	1	2	3	4	5	AVG
1	26.0	25.8	26.3	25.8	25.8	25.9
2	27.9	26.9	26.1	26.3	25.9	26.6
3	26.6	26.8	25.2	25.8	25.7	26.0
4	26.1	26.2	25.6	25.2	24.6	25.5
5	26.8	27.1	26.7	26.4	25.5	26.5
6	26.6	28.0	27.2	26.0	25.5	26.7

While the hardness values of parameter groups 5 and 6 do not exhibit any significant difference, specimens of parameter groups 3 and 2 are harder in comparison to groups 4 and 1, respectively.

4.4. Dome Stretch Test

Table 4.10 shows the LDH values for the 110x110 and 110x75 samples and corresponding force values at yielding. Two samples were tested for each parameter group and for each sample dimension.

Table 4.10. LDH values and corresponding force values at yielding for the dome stretch test specimens.

Sample No	Specimen Dimensions	Parameter Group	Force at Yield (kN)	LDH (mm)
1	110x110	1	13.1	21.1
2	110x110	1	12.7	20.8
3	110x110	2	12.5	20.3
4	110x110	2	12.7	20.6
5	110x110	3	14.1	22.1
6	110x110	3	14.2	22.9
7	110x110	4	13.3	22.3
8	110x110	4	12.8	22.0
9	110x110	5	13.5	22.3
10	110x110	5	13.4	22.3
11	110x110	6	13.5	21.9
12	110x110	6	13.3	21.6
13	110x75	1	13.1	21.3
14	110x75	1	12.6	21.0
15	110x75	2	13.1	20.6
16	110x75	2	12.9	21.2
17	110x75	3	14.5	22.8
18	110x75	3	14.6	23.3
19	110x75	4	13.7	22.7
20	110x75	4	13.7	22.5
21	110x75	5	13.7	22.1
22	110x75	5	13.7	22.2
23	110x75	6	13.6	21.5
24	110x75	6	13.4	21.5

Figure 4.2 shows the averages of the force at yielding and LDH values for each of the parameter groups. A comparison of the groups shows that groups 1-2 and 5-6 do not differ much neither in LDH and force at yielding values. However, looking at groups 3-4, group 3 has significantly larger force at yielding values reaching 1kN, especially for the 110x110 mm specimens.

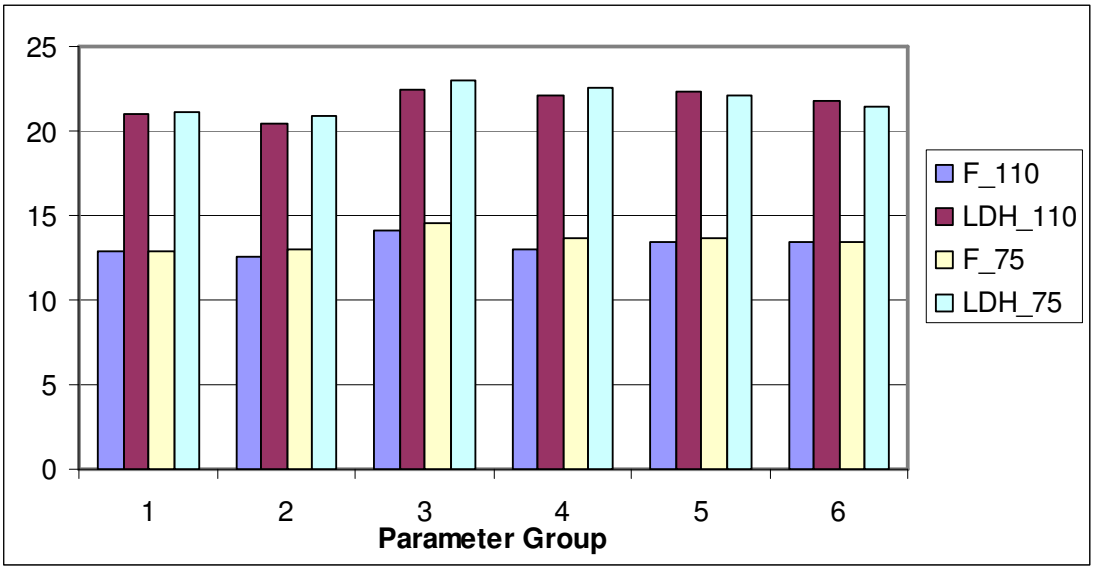

Figure 4.2. Average force at yielding and LDH values for each of the parameter groups.

Figures 4.2 to 4.7 illustrate the FLD's constructed for each parameter group. Local strains were defined as either acceptable (ACC.) in case of no localized necking, or unacceptable (UNACC.) in case of necking and fracture. 4 types of specimens were utilized in forming the diagrams: 110x110, 110x75 and 110x50 dome stretch test specimens, and the uniaxial tensile test specimens. The FLC's were established by connecting the uppermost good major strains over the associated minor strain range. The formation of the FLC was partly based on judgement: There were occasionally acceptable points above the FLC and unacceptable points below the FLC.

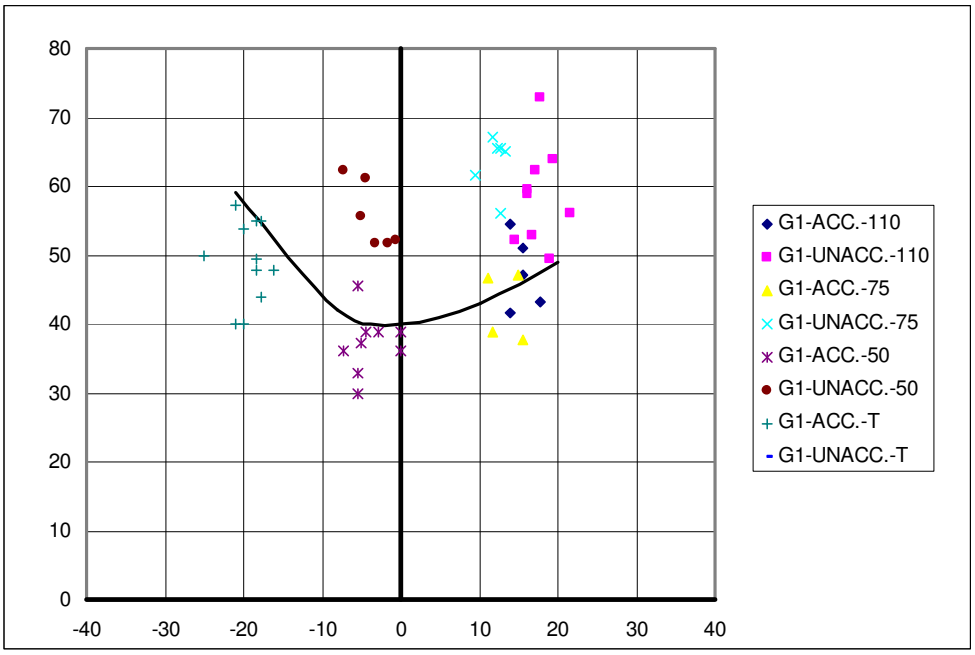

Figure 4.3. FLD for the 1st Parameter Group.

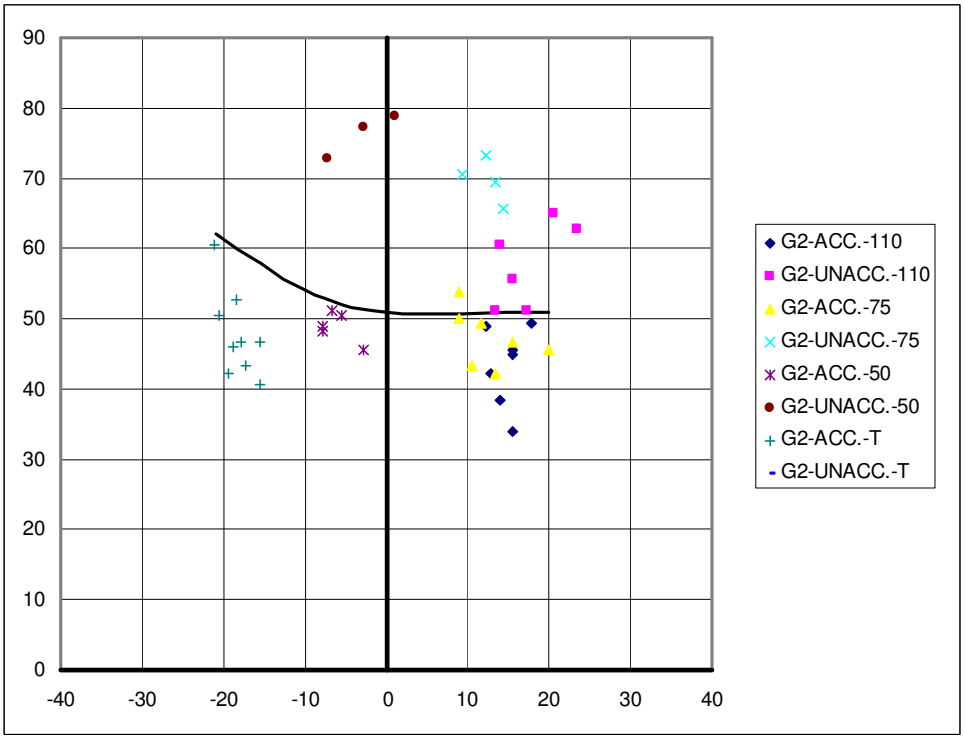

Figure 4.4. FLD for the 2nd Parameter Group.

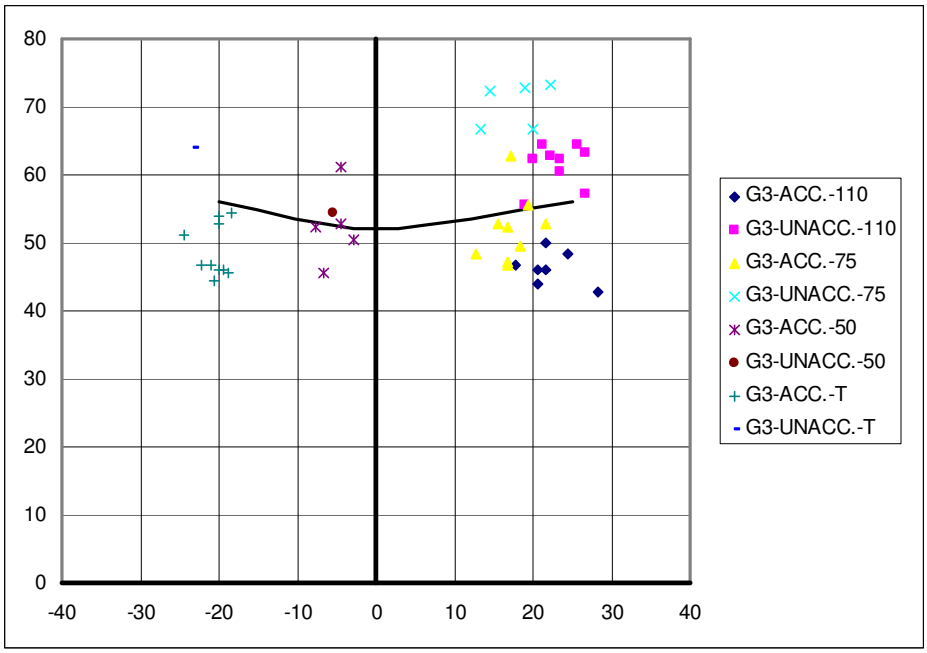

Figure 4.5. FLD for the 3rd Parameter Group.

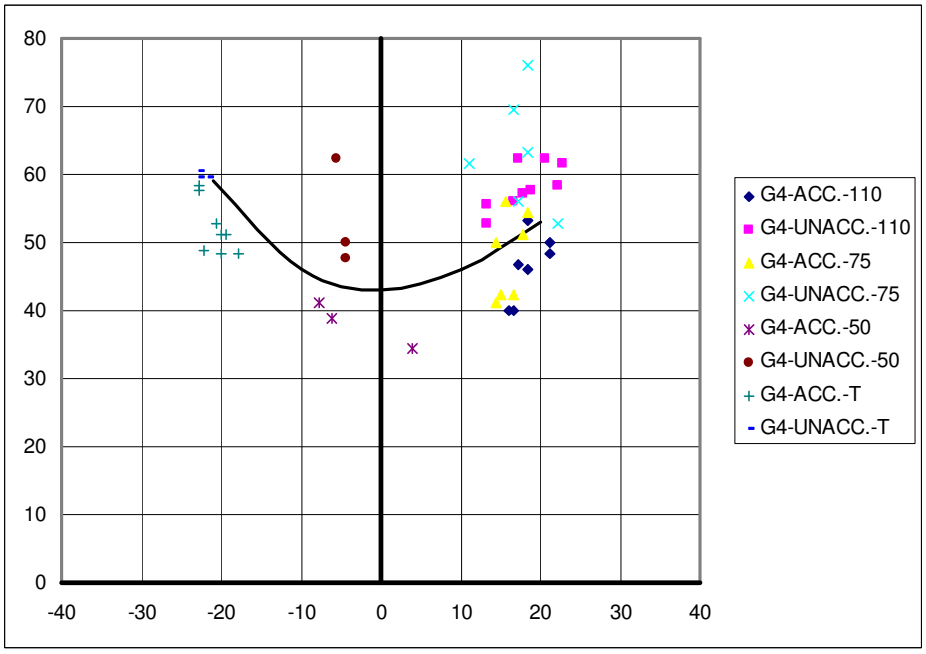

Figure 4.6. FLD for the 4th Parameter Group.

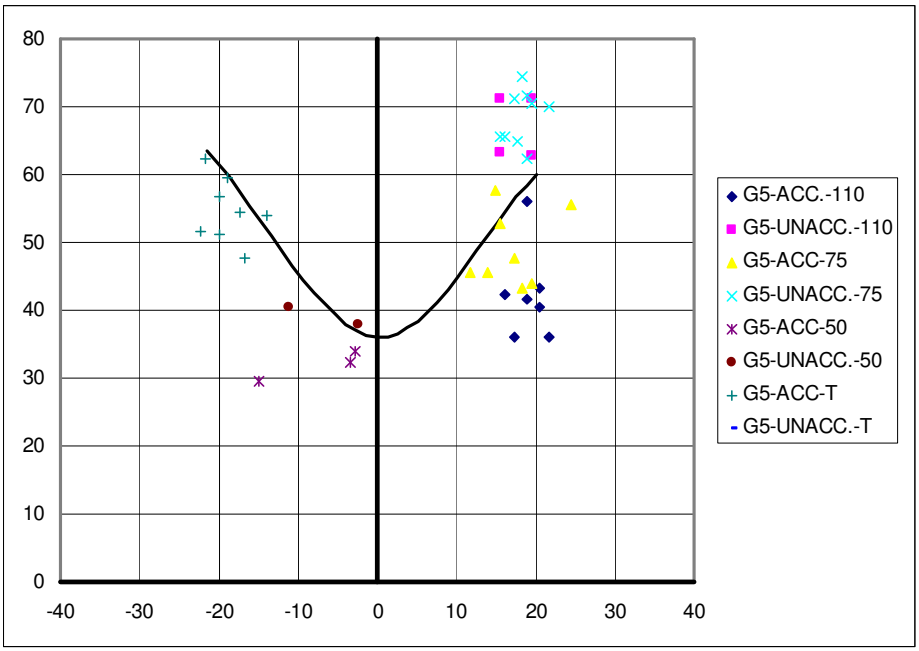

Figure 4.7. FLD for the 5th Parameter Group.

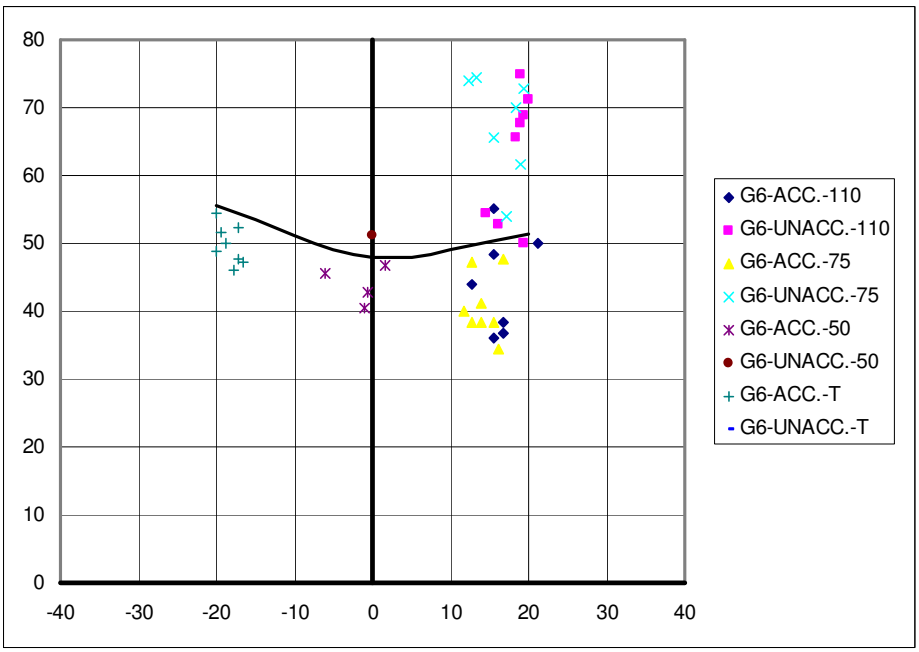

Figure 4.8. FLD for the 6th Parameter Group.

The area under the FLC's in FLD's represent the safety area. Forming operations with local strains in this area are considered as safe, while any strains above the FLC will

cause failure by either localized necking or fracture on the specimen. For the comparison of FLD's of different parameter groups, the areas under the FLC's are taken into account.

An analysis of Figures 4.3 and 4.4 reveals that the area under the FLC of the parameter group 1 covers a wider area than the FLC of the parameter group 2 and thus have better formability. This can be validated by checking the values of uniaxial strain (leftmost strains on the FLD), plane strain (intercept at the major axis) and the biaxial strain (rightmost strains on the FLD). Similarly, the formability performance of parameter groups 3 and 6 are superior to parameter group 4 and 5, respectively.

After the comparisons of parameter groups in pairs, it is appropriate to state that, increasing casting speed impairs the formability behavior, whereas casting with smaller diameter casting rolls and at a decreased casting gauge are advantageous in terms of the formability performance.

4.5. Microstructural Study

Micrographs of the sections transverse to the rolling direction were taken via optical microscope under polarized light at 5x magnification. Figures 4.9-4.14 illustrate the micrographs for the specimens of 6 different parameter groups. In each figure, the picture on the left hand side, (a) represents the as-cast condition of the specimen while the picture on the right hand side, (b) represents the 1,5mm 0-condition of the specimen. The solidification conditions of the as-cast specimens are listed in Table 3.2.

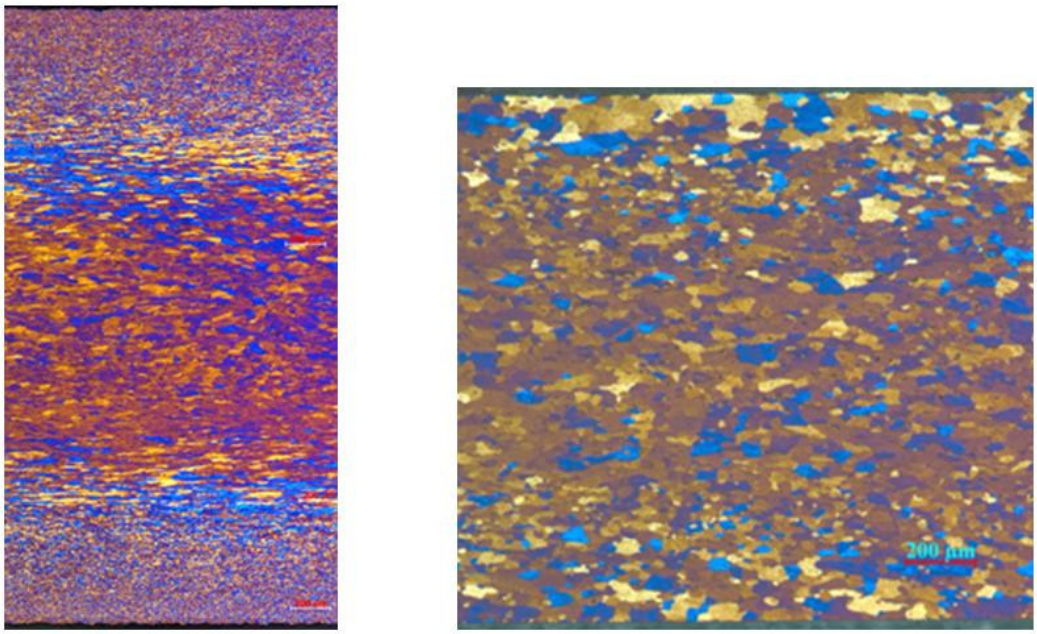

(a) (b)

Figure 4.9. Micrographs of the 1st parameter group specimen. (a) the as-cast specimen, (b) 0-condition specimen.

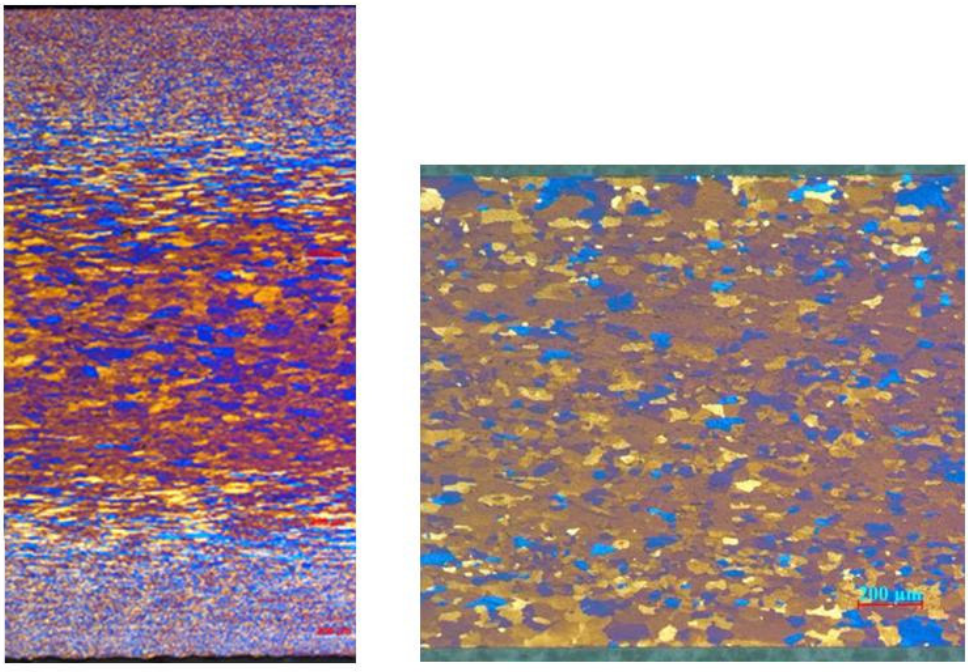

(a) (b)

Figure 4.10. Micrographs of the 2nd parameter group specimen. (a) the as-cast specimen, (b) 0-condition specimen.

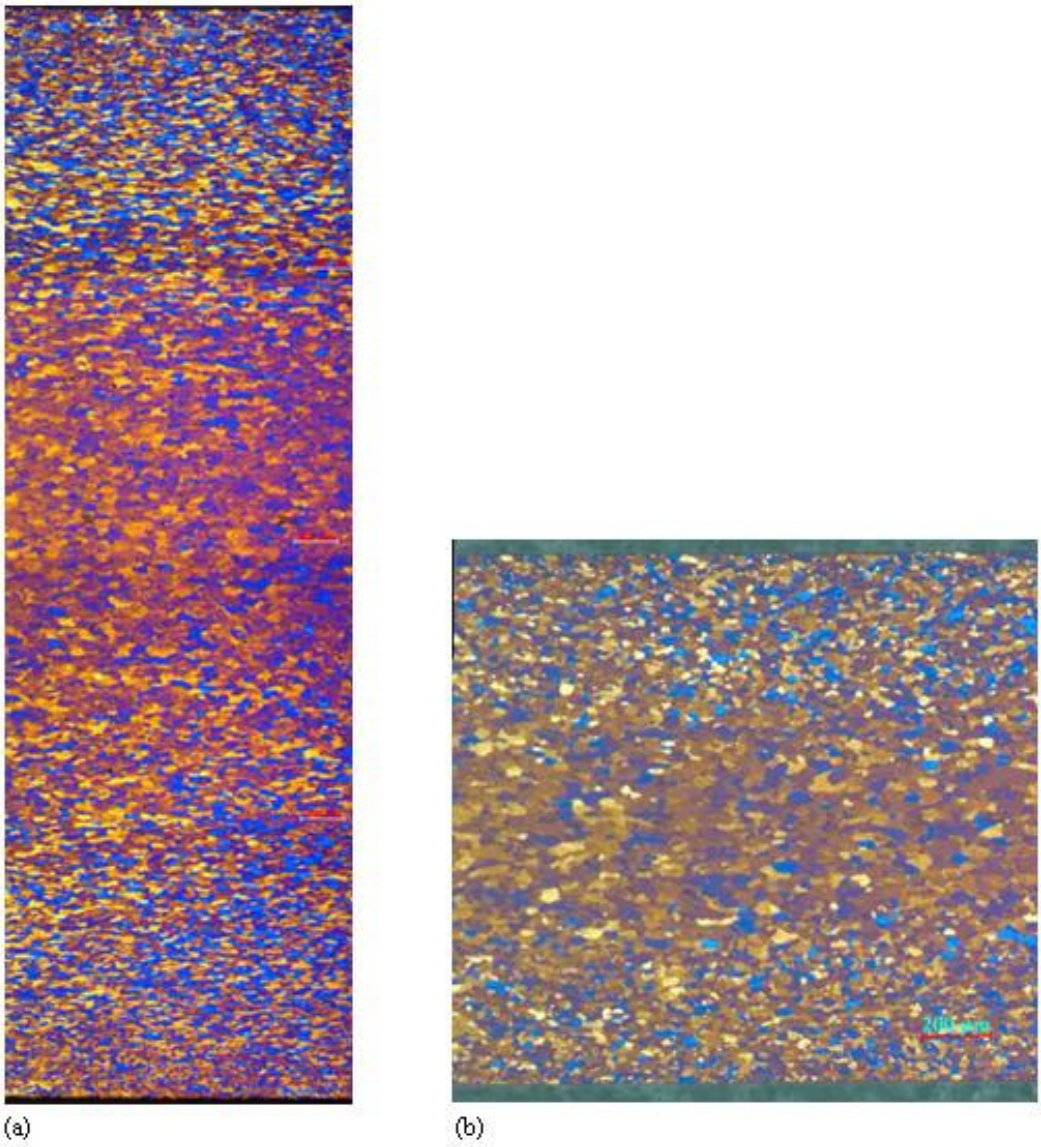

Figure 4.11.Micrograph of the 3rd parameter group specimen. (a) the as-cast specimen, (b) 0-condition specimen.

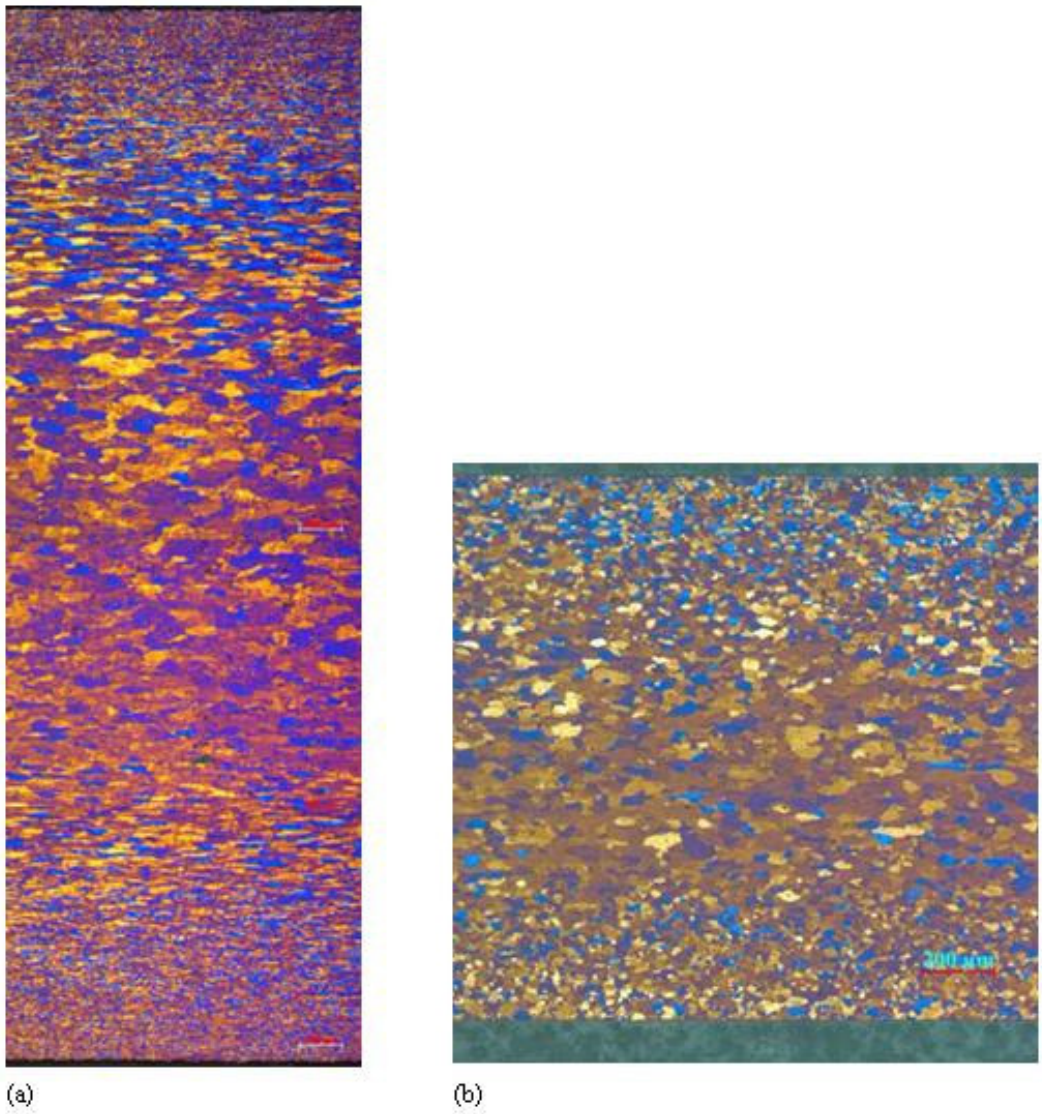

Figure 4.12. Micrograph of the 4th parameter group specimen. (a) the as-cast specimen, (b) 0-condition specimen.

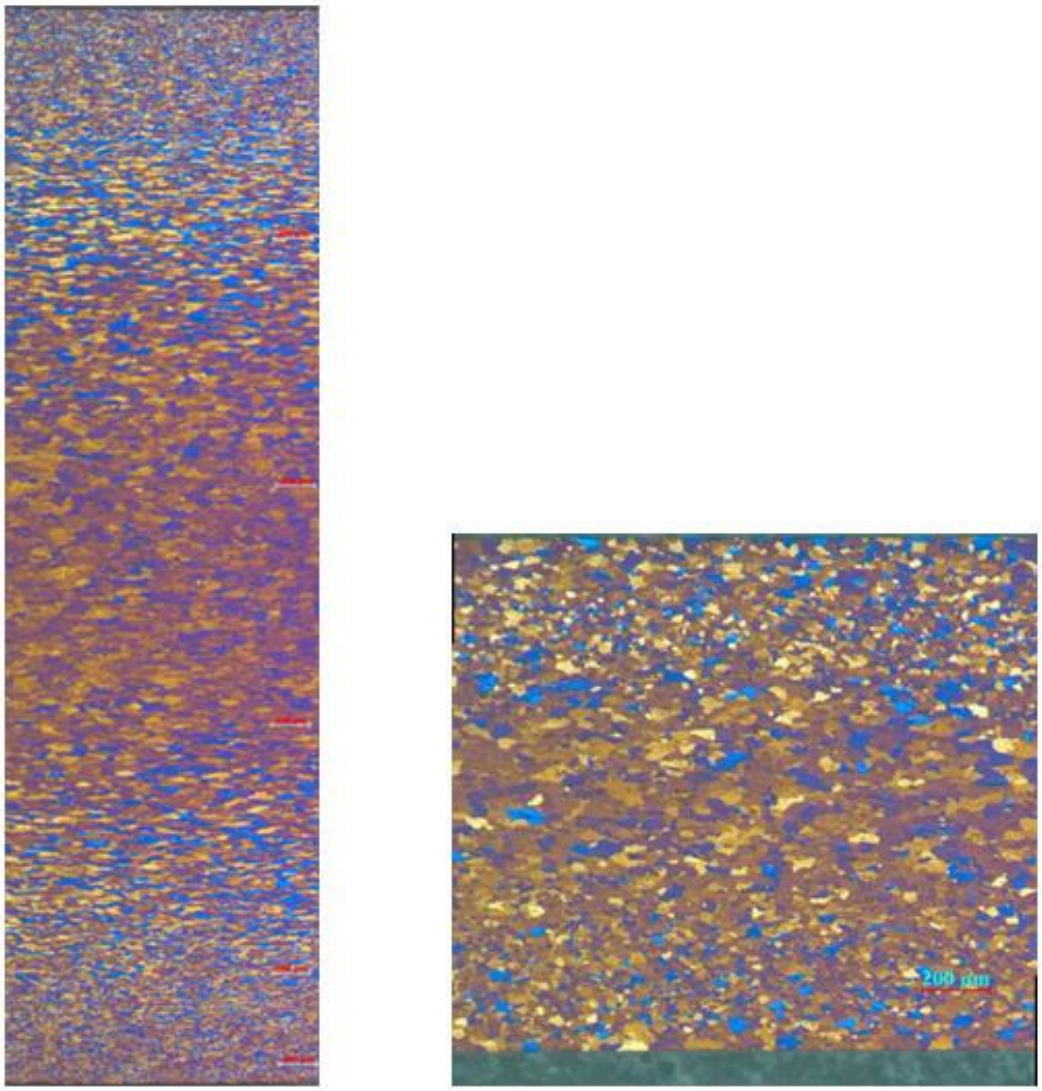

Figure 4.13. Micrograph of the 5th parameter group specimen. (a) the as-cast specimen, (b) 0-condition specimen.

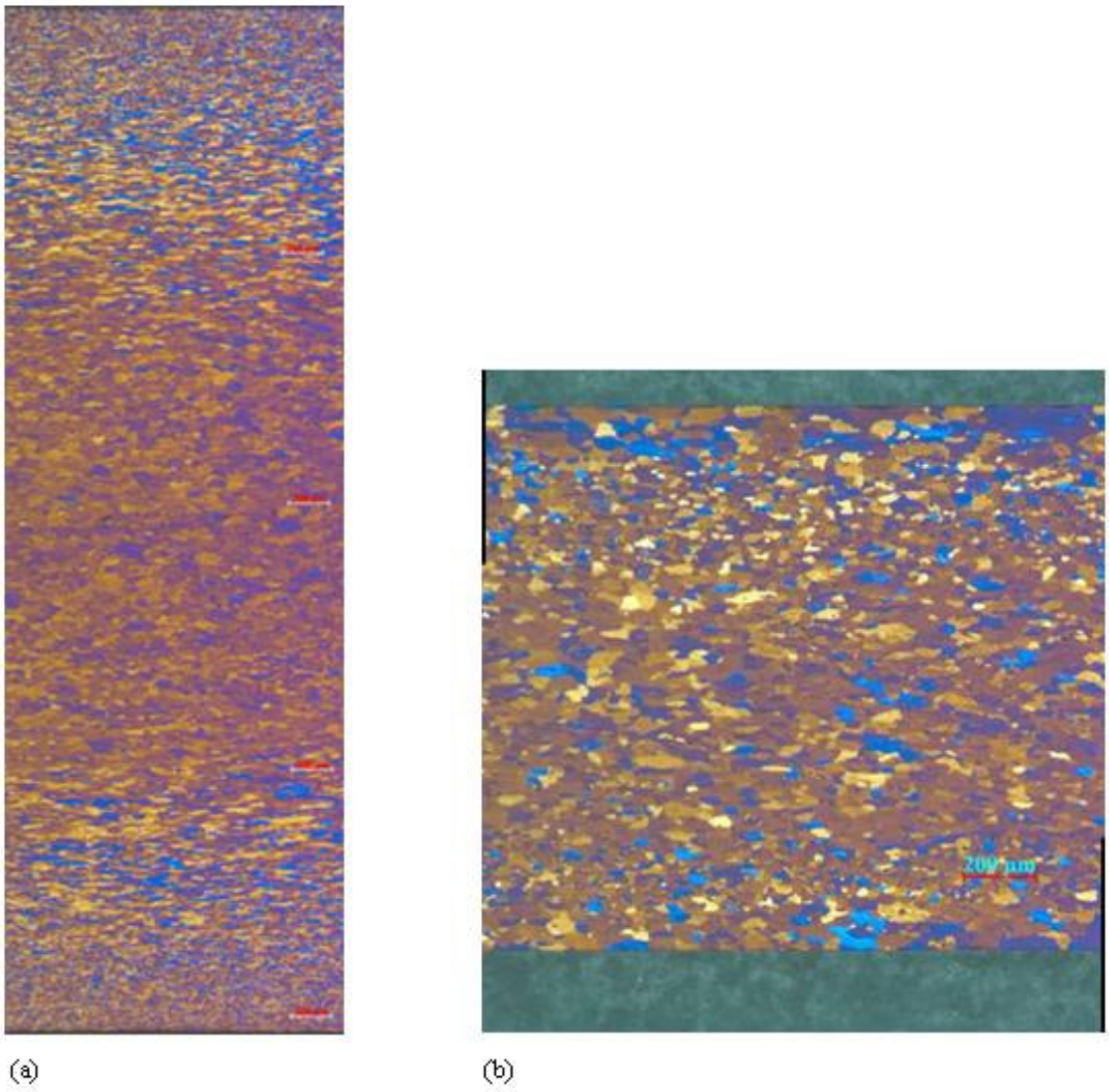

Figure 4.14. Micrograph of the 6th parameter group specimen. (a) the as-cast specimen, (b) 0-condition specimen.

At the first sight to the micrographs of the as-cast specimens, the typical microstructure of a TRC aluminum alloy can easily be seen: Heterogenous grain size distribution throughout the thickness of the specimen and centre line segregations. This heterogeneity is due to the high cooling rate gradient from the surface to the center of the strip. The solidification rate sharply decreases upon development of the first solid layer at the outer skin and the heat flow to the caster rolls then gradually decreases. This leads to relatively coarser particles and larger dendrite arm spacing at some distance from the strip surface.

When the 0-condition, 1.5 mm specimens are inspected, it can be seen that specimens of parameter group 1 and 2 have coarse grains on the surfaces, while groups 3 and 4 have the finest grains, and groups 5 and 6 have in between size grains on the surfaces. The coarse grains of groups 1 and 2 can be explained by the very rapid cooling rates and high deformations encountered in the thin strip casting. Higher cooling rates and deformations tend to form a layer heavily supersaturated with alloying elements and finer grains on the as-cast strip surface. Finer grains and alloying elements increase the stored energy of the metal leading to a faster recrystallization and grain growth.

It should be noticed that the as-cast specimen of parameter group 3 is totally different from the other as-cast microstructures. All other specimens have a large gradient of grain size from the surface to the midsection: a supersaturated region with very small grain sizes on the surface to a region with coarse grains and intermetallic particles. However, with the specimen of parameter group 3, there is a relatively smaller gradient of grain size from surface to the midsection. This is possibly due to the lower cooling rates and separating forces experienced with a smaller diameter casting roll.

4.5.1. Prototype Twin-Roll Caster Samples

Microstructural study was conducted for the AA1050 cast strip obtained from the prototype twin-roll caster. The sample was cast at 690ºC and the thickness is 1.5mm Specimen was sectioned parallel to the rolling direction and cold mounted in bakelite.

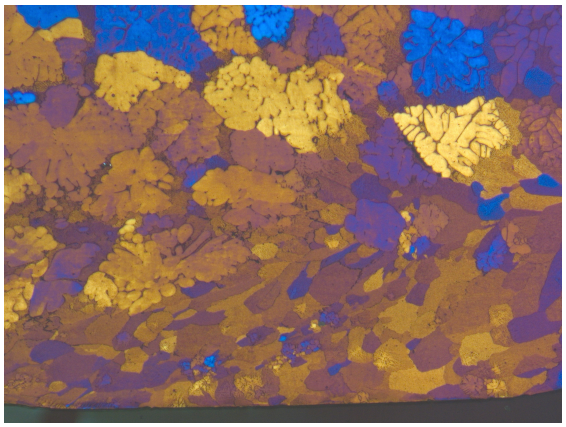

Figure 4.15. Micrograph of the bottom part of the AA1050 alloy cast with the prototype caster. Section is parallel to the rolling direction

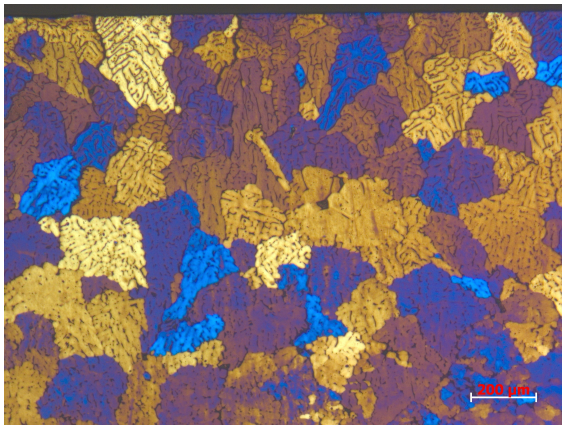

Figure 4.16. Micrograph of the top part of the AA1050 alloy cast with the prototype caster. Section is parallel to the rolling direction

Looking at both Figures 4.15 and 4.16, the average grain size is much larger than the grain sizes of specimens cast at the industrial casters. This is obviously due to the insufficient cooling rate of the casting rolls. Noticeably large spacings between the dendrite arms are another proof of the low cooling rate.

In Figure 4.15, on the bottom surface, smaller grains are elongated in the rolling direction and eutectic structures on the top surface are visible.

5. SUMMARY and CONCLUSIONS

The objective of the current work was to study the effects of three significant solidification parameters, namely the casting speed, the casting gauge and the roll diameter, on the formability behaviour of the twin-roll cast AA1050 sheet.

Both intrinsic tests and simulative tests were performed to assess the formability behaviour of the AA1050 strip. Uniaxial tensile test, Brinell hardness test, dome stretching test and Erichsen test were performed. Since the formability of a sheet metal depended primarily on its crystallographic texture and grain size, a microstructural study was also performed to the as-cast and annealed samples.

The results of the uniaxial tensile test showed that $\bar{n}$ values did not exhibit a significant change with the variation in any of the solidification parameters. Larger uniform elongation values were obtained by increasing the casting gauge. Δr values closer to 0 and r_m values closer to 1 were recorded using increased casting speed and roll diameter, respectively.

The results of the Erichsen test and the Brinell hardness test did not provide much of an insight to understanding the change of formability behaviour under different solidification conditions. For the Erichsen test, it was only the increase of the roll diameter which resulted in the decrease of stretchability. For the Brinell hardness test, increasing the casting speed yielded slightly harder specimens, whereas an increased roll diameter produced softer specimens.

Forming limit diagrams (FLD) were constructed from an array of dome stretching test specimens by using grid strain analysis. Limiting dome heights (LDH) and forces at yield points were also measured. Inspection of the FLD's showed that the area under the forming limit curves decreased with increased casting speed, casting gauge and roll diameter. In addition, specimens cast at increased roll diameters yielded at smaller forces.

Microstructural study of the as-cast samples showed heterogenous grain size distribution throughout the thickness of the samples and centre line segregations. However, with decreased roll diameter, a significantly less heterogenous microstructure was attained. This was possibly due to the lower cooling rates and separating forces experinced with a smaller diameter casting roll.

When the microstructures of the annelead samples were inspected, it was seen that 3mm cast specimens had the most coarse grains on the surfaces, which can be explained by the very rapid cooling rates and high deformations encountered in the thin strip casting.

Within the scope of the current work, the existing hot rolling machine in the Materials Laboratory was revised into a twin-roll caster. Casting trials were performed and microstructural studies were conducted on the as-cast samples. It was seen that the average grain size of the samples cast at the prototype caster was much larger than the grain sizes of specimens cast at the industrial casters. This was obviously due to the insufficient cooling rate of the casting rolls.

REFERENCES

1. Sanders, R.E., "Technology Innovation in Aluminum Products", The Journal of The Minerals, Metals & Materials Society, Vol. 2, pp. 21-25, February 2001.

2. Dong-Ying, J. and H. Xiao-Dong, "Effect of Casting Parameters and Deformation on Microstructure Evolution of Twin-Roll Casting Magnesium Alloy AZ31", The Transactions of Nonferrous Metals Society of China, Vol. 16, pp. 874-877, June 2006.

3. Ertan, S., M. Dündar, Y. Birol, and K. Sarıoğlu, "The Effect of Casting Parameters on Twin Roll Cast Strip Microstructure", Proceedings of the Light Metals, pp 667-672, 2000.

4. Sommerhofer, H., "Influence Parameters on Continuous Casting of Aluminum", Light Metals, Vol. pp. 733-740, 2003.

5. Vangala, P., D. Smith, R. Duvvuri, and C. Romanowski, "The Influence of Casting Gauge on the Hunter Roll Casting Process", Melt-spinning and Strip Casting: Research and Implementation, pp. 333-347, The Minerals, Metals & Materials Society, California, 1992.

6. The Economist, "Economic and financial indicators", Dec 10, 2006.

7. World Aluminium, http://www.world-aluminium.org, Primary Aluminum Production, 2006.

8. Alüminyum İstatistikleri, http://www.aluminyumsanayi.com/istatistik.html, Türkiye Alüminyum Sektörü, 2005.

9. Kalpakjian, S. and S.R. Schmid, Manufacturing Engineering and Technology, Prentice Hall International, 2000.

10. Smith, W.F., Principles of Materials Science and Engineering, McGraw-Hill, 1986.

11. Slamova, M., M. Karlık, F. Robautc, P. Slama, and M. Veron, "Differences in Microstructure and Texture of Al–Mg Sheets Produced by Twin-Roll Continuous Casting and by Direct-Chill Casting", Materials Characterization, Vol. 49, pp. 231-240.

12. AluMatter, Processing of Aluminium, http://aluminium.matter.org.uk, 2006.

13. ASM Handbook, Molding and Casting Processes, 2003.

14. Menet, P.-Y., F. Basson, K. Maiwald, R. Cayol, and M. Bosch, "Strip Casting Technology… A Key to Product Quality", Proceedings of the International Melt Quality Workshop, Madrid, 2001.

15. U.S. Pat. 6,672,368 (February 19, 2002), Ünal, A.

16. Haga, T. and S. Suzuki, "Roll Casting of Aluminum Alloy Strip by Melt Drag Twin Roll Caster", Journal of Materials Processing Technology Vol. 118, pp. 165-168.

17. Suzuki, K., S. Kumai, Y. Saito, and T. Haga, "High-Speed Twin-Roll Strip Casting of Al-Mg-Si Alloys with High Iron Content", Materials transactions, Vol. 46, pp. 2602-2608, 2005.

18. Alper, G., Alüminyum Sürekli Döküm Yöntemi ile Üretilmiş 5052-5182 Alüminyum Alaşımlarının Şekillendirilebilirlik Kabiliyetlerinin Belirlenmesi, M.S. Thesis, İ.T.Ü., 2003.

19. U.S. Pat. 48,053 (July 25, 1865), Bessemer, H.

20. U.S. Pat. 2,790,216 (April 30, 1957), Hunter, J.L.

21. U.S. Pat. 5,518,064 (May 21, 1996), Romanowski, C., et al.

22. U.S. Pat. 4,409,027 (June 28,1982), Cordea, J.N. and H.V. Sheth.

23. U.S. Pat. 5,531,659 (February 14, 1995), Fusada, T.

24. Dündar, M., A.S. Akkurt, K. Sarıoğlu, and C. Romanowski, "The Influence of Caster Roll Diameter on the Microstructure of Twin Roll Cast Aluminum Strip", Proceedings of the Light Metals, pp 719-724, 2003.

25. Pyrotek, Casting Tips, http://www.pyrotek-inc.com, 2002.

26. Berg, B.S., V. Hansen, P.T. Zagierski, M.L. Nedreberg, and A. Olsen, "Gauge reduction in Twin-Roll Casting of an AA5052 aluminium alloy: The effects on microstructure", Journal of Materials Processing Technology Vol. 53, pp. 65-74.

27. Doğan, N., Hunter Sürekli Döküm Prosesi ile Üretilen Al-Fe-Mn-Si Alaşımının Mikroyapısının Karakterizasyonu ve Mekanik Özelliklerinin Belirlenmesi, M.S. Thesis, İ.T.Ü., 1998.

28. Bayraktar, E., Deformation Behaviour and Formability Characterization of Hadfield Steel, Ph.D. Thesis, Bogazici University, 1993.

29. AluMatter, Forming: Introduction and Definitions, http://aluminium.matter. org.uk/, 2006.

30. ASM Handbook, Forming of Nonferrous Sheet Materials, 2003.

31. ASM Handbook, Evaluation of Formability for Secondary (Sheet) Forming, 2003.

32. Schey, J.A., Introduction to Manufacturing Processes, pp. 408, McGraw Hill, New York, 2000.

33. Han, J.-H., H.-K. Seok, Y.-H. Chung, M.-C. Shin, and J.-C. Lee, "Texture evolution of the strip cast 1050 Al alloy processed by continuous confined strip shearing and its formability evaluation", Materials Science and Engineering A323, Vol. pp. 342–347, 2002.

34. Haberfield, A.B. and M.W. Boyles, Laboratory Determined Forming Limit Diagrams, Sheet Metal Industries, pp 400-405, 1973.

35. Rees, D.W.A., "Factors influencing the FLD of automotive sheet metal", Journal of Materials Processing Technology Vol. 118, pp. 1-8, 2001.

36. The_Aluminum_Association, International Alloy Designations and Chemical Composition Limits for Wrought Aluminum and Wrought Aluminum Alloys, pp 2004.

37. ASTM Standard E-8, "Standard Test Methods for Tension Testing of Metallic Materials", 2004.

38. ASTM Standard E-2218, "Standard Test Method for Determining Forming Limit Curves, 2002.

39. ASTM Standard E-517, "Plastic Strain Ratio r for Sheet Metal", 1981.

40. Bacroix, B., T. Chauveaua, J.F. Duarte, A.B.d. Rocha, and J. Gracio, "The respective influences of grain size and texture on the formability of a 1050 aluminium alloy", International Journal of Engineering Science, Vol. 37, pp. 509-526.

41. Deublin Company, Rotating Union Applications, http://www.deublin.com/products/union.asp, 2006.

42. SKF, Spherical Roller Bearings, http://www.skf.com, 2006.

APPENDIX

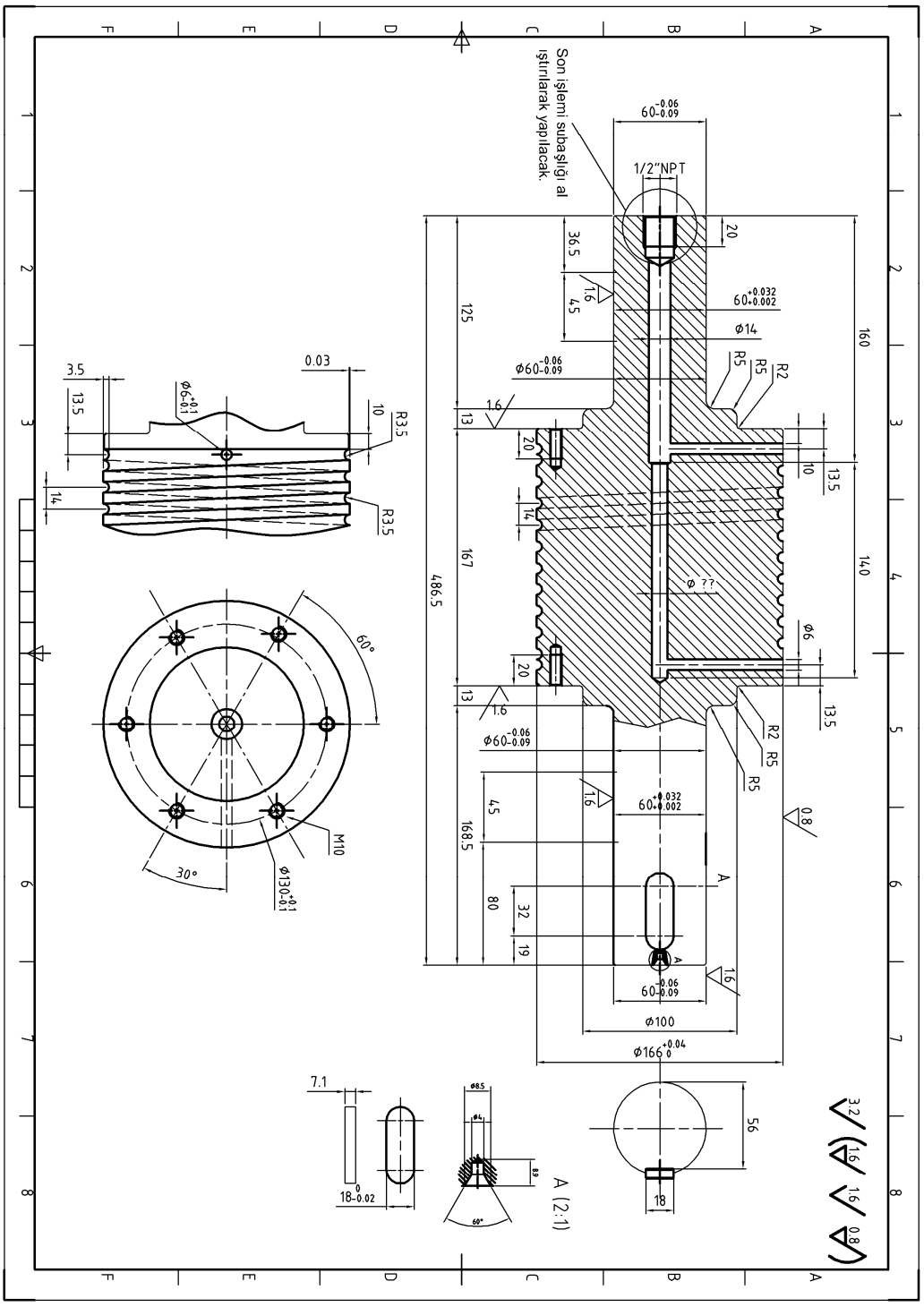

Figure A.1. Core of the prototype twin-roll caster

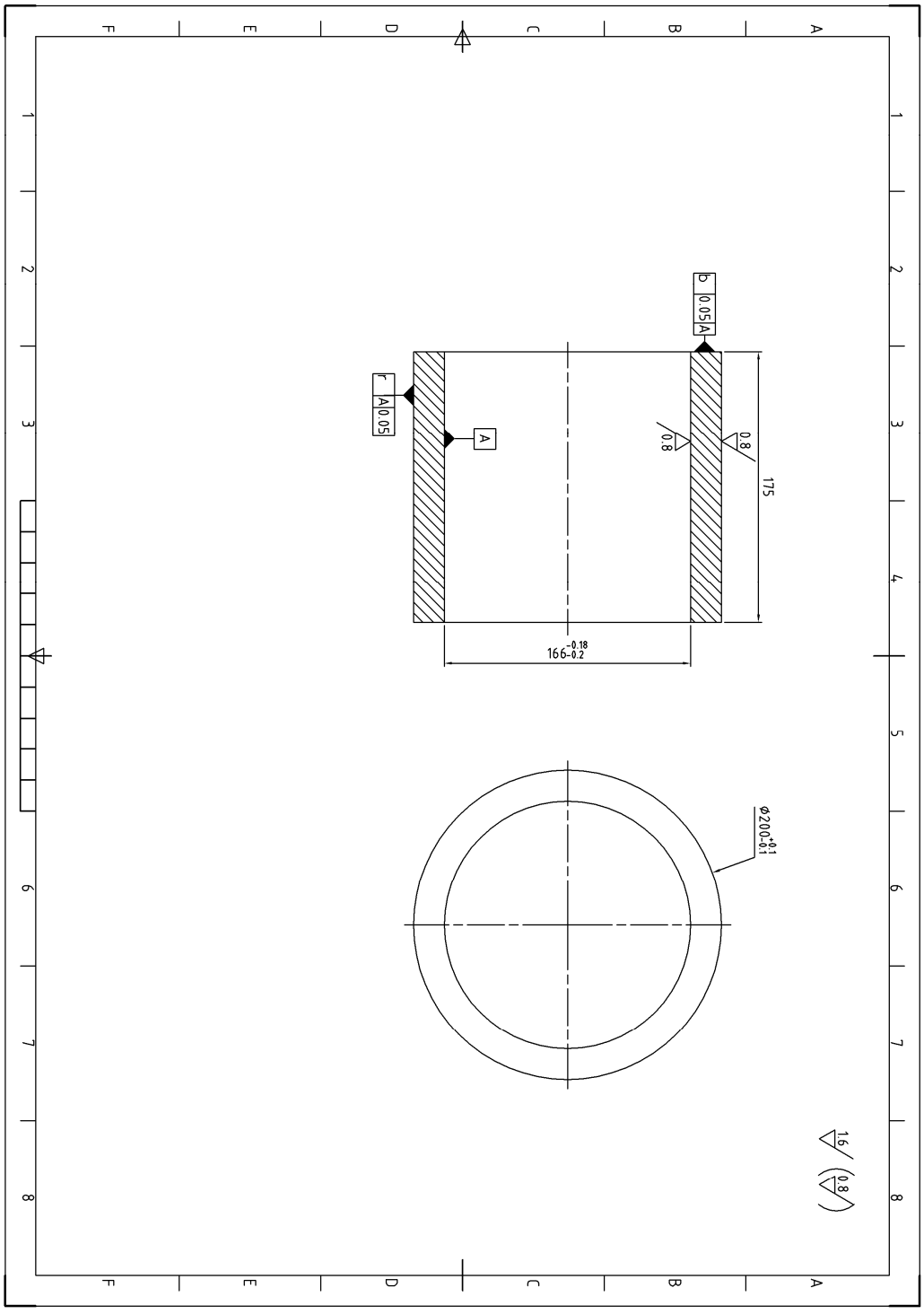

Figure A.2. Shell of the prototype twin-roll caster

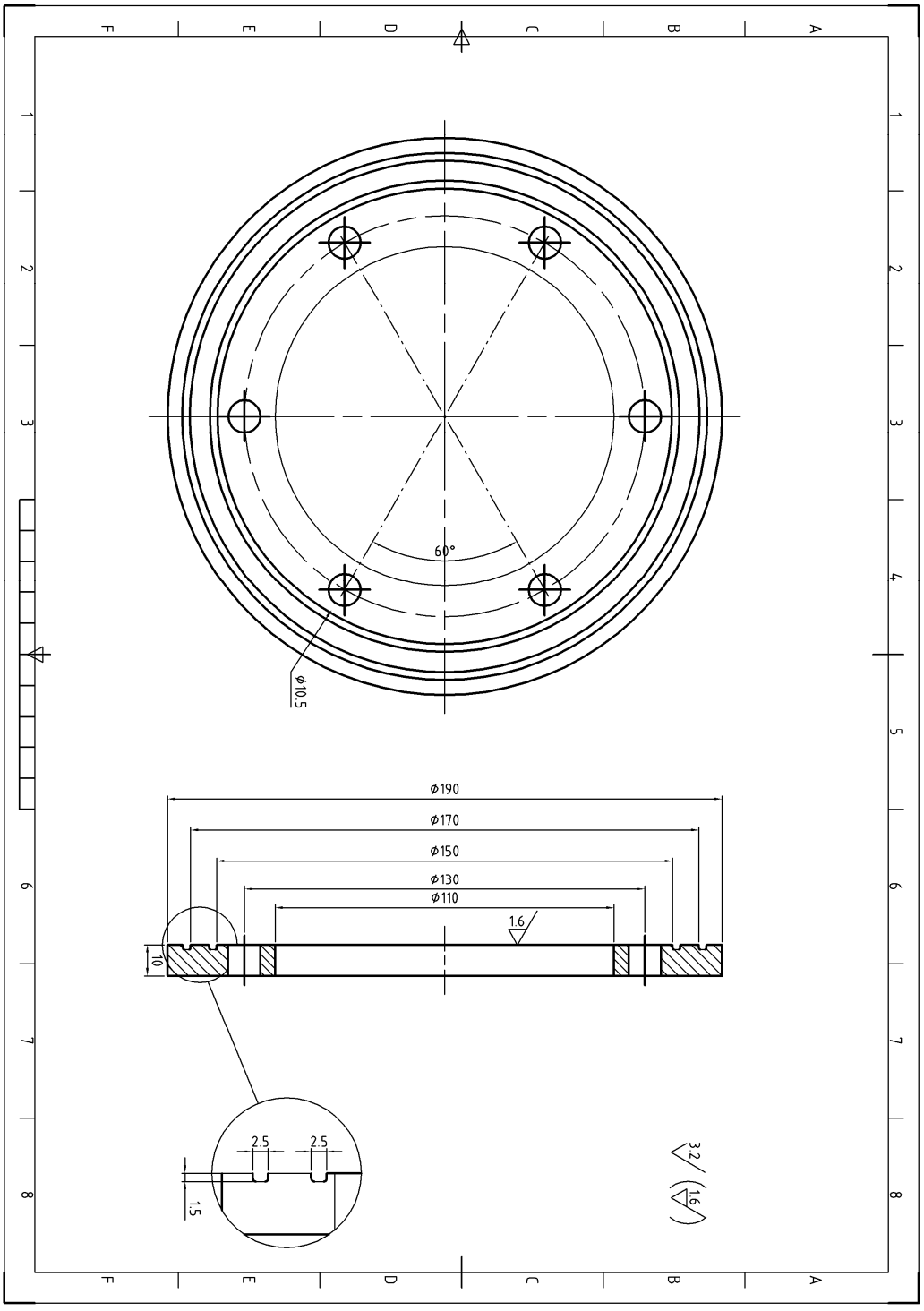

Figure A.3. Flange of the prototype twin-roll caster

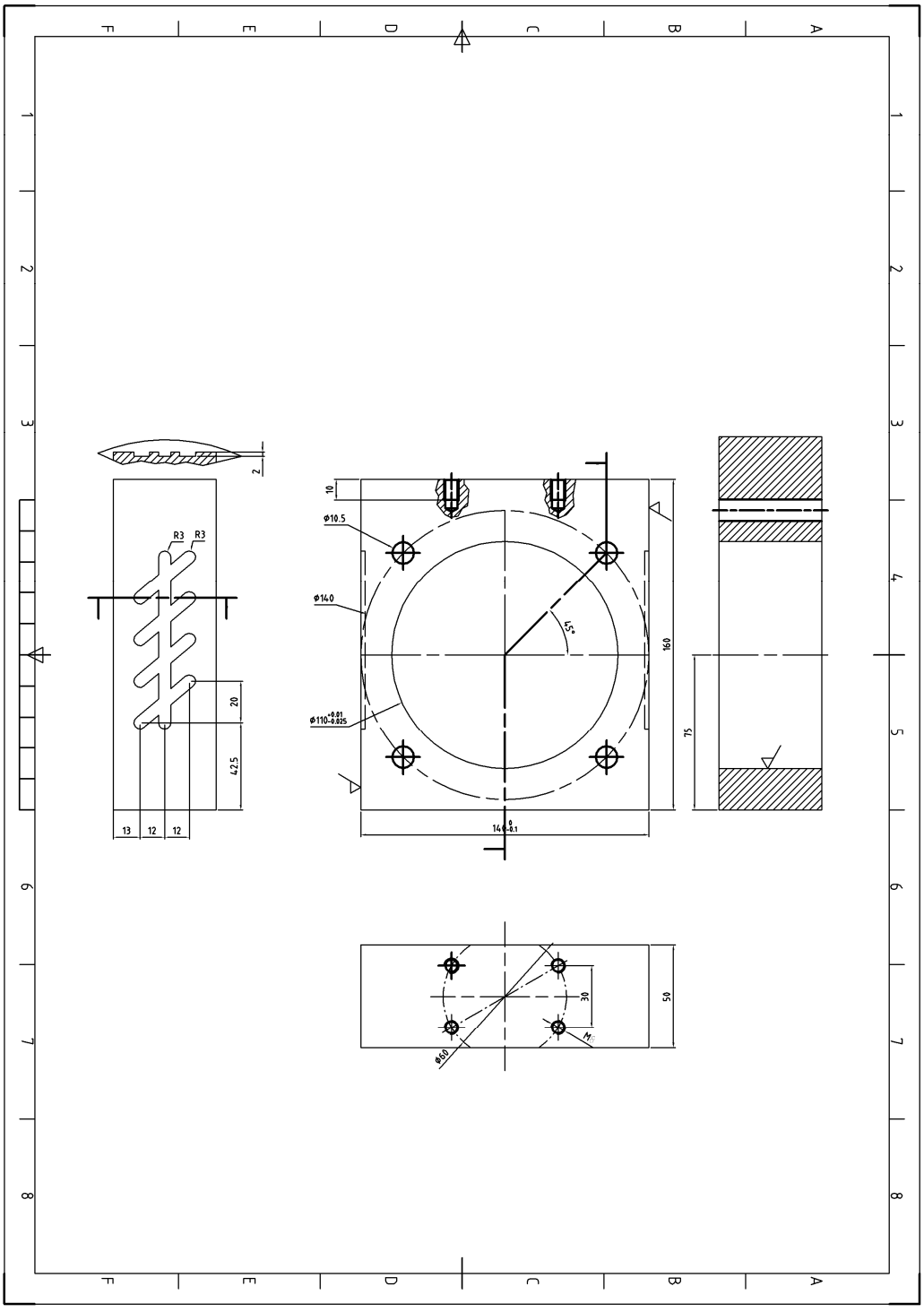

Figure A.4. Housing of the prototype twin-roll caster

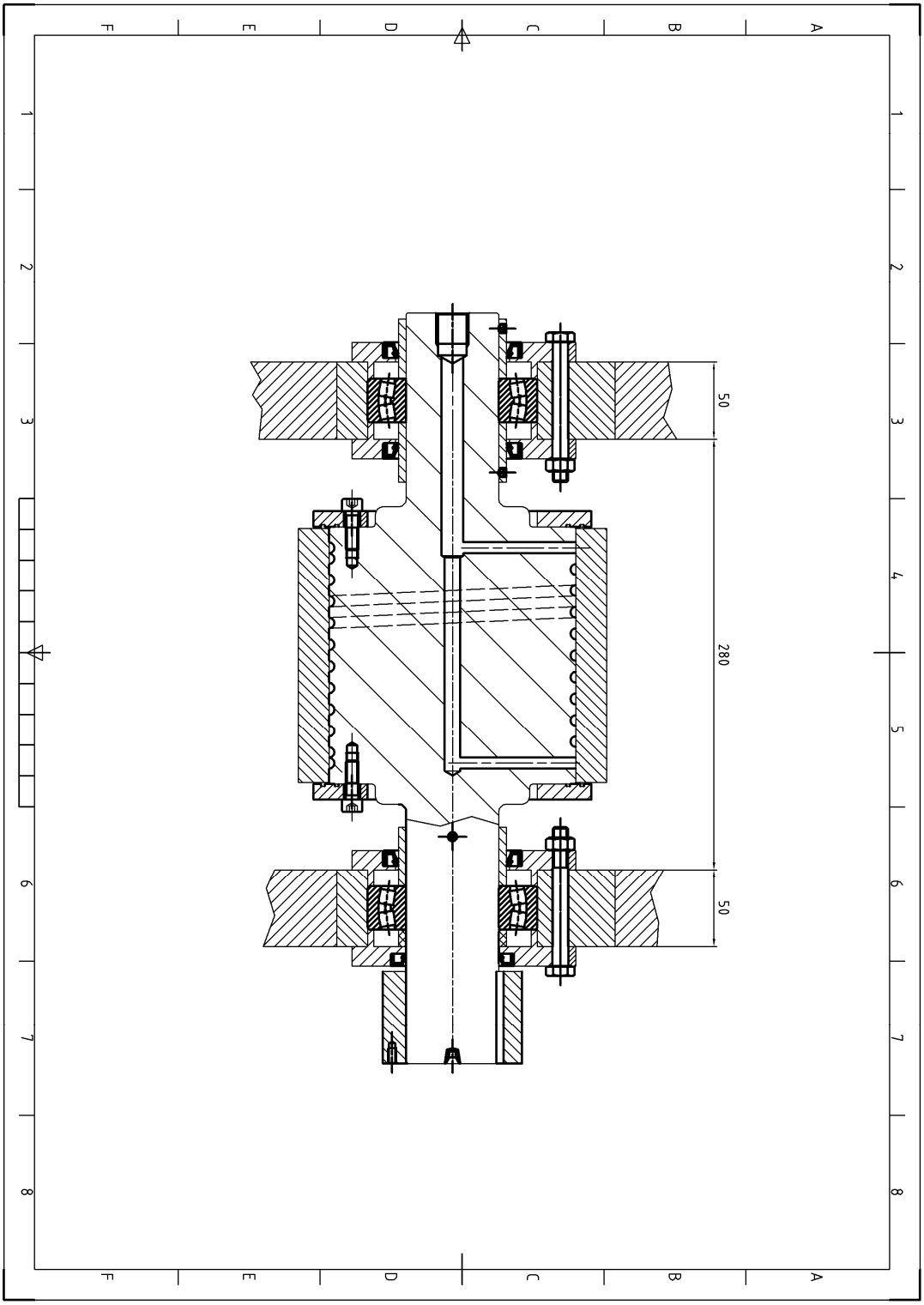

Figure A.5. Core and shell assembly

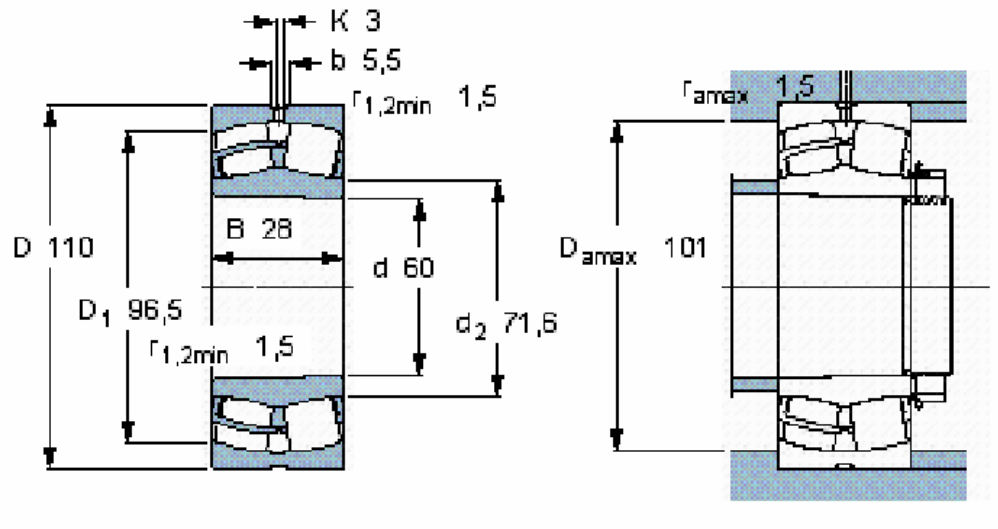

Figure A.6. Spherical roller bearings [42]